Long Range Outlook for Short-Range Correlations

N. Fomin,[1] D. Nguyen,[1] J. Kahlbow,[2] D. Nguyen,[1] J. Pybus,[3] N. Rocco,[4]
M. Sargsian,[5] S. N. Santiesteban,[6] R. Weiss,[7] and Your Name[8]

[1] *University of Tennessee, Knoxville, TN 37996, USA*
[2] *Lawrence Berkeley National Laboratory, Berkeley, CA 94720, USA*
[3] *Los Alamos National Laboratory, Los Alamos, NM 87545, USA*
[4] *Argonne National Laboratory, Lemont, IL 60439, USA*
[5] *Florida International University, University Park, Florida 33199, USA*
[6] *University of New Hampshire, Durham, NH 03824, USA*
[7] *Washington University in Saint Louis, Saint Louis, MO 63130, USA*
[8] *Prestigious Institution*

(Dated: March 7, 2025)

I. INTRODUCTION

A short-range correlation (SRC) is a configuration of 2+ nucleons in a nucleus with large relative momentum ($p_{rel} > p_{fermi}$) and smaller center of mass momentum.

A Brief History The story of SRCs begins earlier than most people realize, reaching back into the 1950s. The shell model of Geoppert and Mayer and Jensen [1] described independent particles moving in a mean field and is what most of us think about when we think of "mean field". Later, the addition of vibrational and rotational excitations of nuclei via the time evolution of a self-consistent mean field provided a unified description of single-particle and collective degrees of freedom in nuclei. However, this did not yet include high-momentum nucleons (with momenta above Fermi momentum).In 1955, Brueckner [2] considered nonlinear phenomena in strong short-range interactions. They analyzed several high-energy reactions showed that the measured cross sections can only result from momentum distributions with significant high-momentum tails. This was the first implication for correlations in the nuclear ground-state wave function. Bruckner explains it in the context of strong short-range repulsion in the NN interaction, which also explained s-wave phase shift turning negative at high energies. At this stage, the shell model is considered only approximately correct.

In the following decades, new theoretical approaches were introduced and experimental data lepton scattering and hadronic probes poured in, enriching and sometimes challenging our understanding.

In this paper, we will review and summarize advances in theory and experiment starting in the "modern" SRC era. While SRCs have been proposed as a contributing factor to or a cause of many other observed phenomena, we focus on the SRCs themselves. While our understanding has grown by leaps and bounds since the 1950s, there are still unanswered questions and we aim to identify those and propose a path to answer them.

II. PROBING CORRELATIONS [THEORY AND EXPERIMENT]- UNTIL 2005-2010

The rationale of probing short range nuclear correlations is due to the expectation that the large overlap between constituent nucleons in nuclei is conducive for probing onset of QCD dynamics between overlapped nucleons. There are many questions that such a study can answer, for example, whether two overlapped nucleons collapse to the six-quark state or the transition happens gradually with the enhanced role of quark-interchanges between these nucleons; will such a transition happen through the enhancement of non-nucleonic baryonic components such as $N\Delta$, N, N^*, $\Delta\Delta$, and will the strangeness play a role? The other important issues are the existence of pure QCD degrees of freedom in these states such as hidden-color and quark-anti-quark components. Understanding the transition mechanisms to non-nucleonic components and evaluating their strength at short distances will also contribute to the progress of understanding the dynamics of super-dense nuclear matter that may exist in the cores of neutron stars or generated during the merger of neutron stars.

Probing the short range configurations in the momentum space is related to the probing nucleons with *large relative momenta* in the nucleus. The probability amplitude of finding bound nucleon with large momentum is the part of the high momentum component of the nuclear wave function. Thus one of the main research goals is the study of the structure of nuclear wave function with large momenta of its constituents. Phenomenologically, these studies aim at probing bound nucleon with momenta exceeding characteristic Fermi- momentum in the nucleus ($k_{Fermi} \sim 250 - 300$ MeV/c for medium to large nuclei). During the last two decades, both theoretical and experimental investigations reached up to the $\sim$ 600 MeV/c nuclear wave function, with rather good understanding of its composition and dynamics.

A. Can we probe SRCs?

Unlike cross sections and energies, wave functions and the nuclear Hamiltonian (or the nuclear interaction) are not observables. Different wave functions and consistent Hamiltonians can reproduce exactly the same experimental data. This can be seen by the fact that a unitary transformation $\hat{U}$ can change the wave function and relevant operators without changing matrix elements (that correspond to observables) [3]:

$$\langle \Psi_f | \hat{O} | \Psi_i \rangle = \langle \hat{U} \Psi_f | \hat{U} \hat{O} \hat{U}^\dagger | \hat{U} \Psi_i \rangle. \tag{1}$$

Specifically, similarity renormalization group evolution can significantly change the short-range (or high-momentum) components of the wave function. Thus, strictly speaking, momentum distributions, the number of high-momentum particles, or the existence of large short-range correlations are not observables and cannot be measured in experiments.

Specifically, SRC experiments are traditionally interpreted assuming high resolution interactions, i.e., nucleon-nucleon interactions with a significant repulsive hard core at short distances.In this case, the reaction is dominated by a one-body current which knocks out a nucleon from the system. In this resolution, ignoring for now caveats related to, e.g., final-state interaction, one can extract from experiments the energy-momentum distribution of nucleons in the ground state wave function. In turn, one can use this information to calculate other quantities and observables. But, this must be done in a consistent way. For example, if momentum distribution of a nucleus is extracted from experiment in this way, and one would like to use this information to calculate the ground-state energy of this nucleus, it must be combined with the same original interaction model used in the analysis of the experimental data. Using this information in a different resolution requires appropriate evolution [3].

In this paper, statements regarding the extraction of SRC properties or momentum distributions from experiments, or regarding the impact of specific features of the nuclear force (like hard repulsive core) on cross sections should be understood in this context. These statements are resolution dependent, but can still be useful, as discussed above. We will also discuss here other interpretations of the same experimental data, involving only low-momentum particles but a different reaction mechanism [4].

The inclusive scattering from any nucleus is driven by scattering from 2N-SRCs, requiring that x and Q^2 be large enough to forbid scattering from nucleons below the Fermi momentum. Scattering in this region should therefore exhibit a universal behavior, resulting in a nuclear cross-section ratio in the SRC-dominated region that is independent of both x and Q^2. The experimental evidence supporting this prediction comes from SLAC [5], which observed a plateau in the σ_A/σ_D cross-section ratio for $x > 1.4$ and $Q^2 > 1.4$ GeV^2 for ^{3}He, ^{4}He, ^{12}C, ^{27}Al, ^{56}Fe, and ^{197}Au. SLAC analysis also showed for the first time the scaling behavior in the LC variables α (light-cone nuclear momentum fraction carried by the struck nucleon). Scaling sets in at $\alpha = 1.25$ to 1.3, providing evidence for the dominance of nucleons with $k > 0.3$ GeV. They assumed that the FSI between the outgoing nucleons of the SRC is proportional to the internucleon wave function at short distances, and thus only weakly depends on the nuclear environment. Therefore, FSI effects are canceled out in the cross-section ratios when the motion of the pair in the mean field is ignored.

Two body breakup measurements were performed using both proton and electron probes to study the isospin structure of NN-SRC pairs. In this reaction, a high-energy proton (electron) scattered off a nucleon in 2N-SRC pairs. High-momentum knocked-out protons and recoiled proton/neutron with similar momentum in the opposite direction are detected. The proton scattering measurement on the Carbon target at BNL showed that the removal of a proton from nuclear with initial momentum 275-550 MeV/c is 92^{+8}_{-18}% of the time accompanied by emission of the correlated neutron that carries momentum equal and opposite to initial proton momentum[6]. This is the first evidence of np dominant in 2N-SRCs and it agrees well with the prediction from the theory calculation.

Independent measurement using electron scattering was performed at Jefferson Lab on Carbon in 2008. The results indicate that $96 \pm 22\%$ of $(e, e'p)$ events with knocked-out protons with initial momentum above 300 MeV/c had a recoiled neutron with similar momentum and in the opposite direction. This ratio for recoiled proton is $9.5 \pm 2\%$. This result showed that almost all high momentum protons have a correlated nucleon and that nucleon is almost always a neutron. The number of SRC np pairs is nearly 20 times more than SRC pp pairs and, by inference, the nn pairs [7]. This result is consistent with the proton scattering measurements. The agreement from two independent probes demonstrates the nature of isospin dependence, np-dominant of 2N-SRCs pairs.

B. High-resolution structure calculations of SRCs

Short-range correlations, induced by the nuclear interaction at short distances, have an impact on various ground-state quantities. Most clearly identified are high-momentum tails of different momentum distributions, that do not exist in mean-field models. Similarly, significant depletion in two-body densities at short distances can be attributed to a short-range repulsion in nuclear interactions (for high-resolution interaction models).

Different studies have focused on ab-initio calculations of such features. Calculations have been performed using quantum Monte Carlo methods, the hyperspherical harmonics method, Green's function approach, and others. Calculations of one-body momentum distributions show high-momentum tails extending well beyond the Fermi momentum [8–14]. It is also seen that the shape of such tails is similar to the deuteron's high momentum tail, indicating that high momentum nucleons are created due to two-body effects (deviations are seen due to the impact of non-deutron-like pair [8–10]). Similar observation is seen for the two-body distributions at short-distances and high-momentum [8, 13, 15, 16]. Calculations of two-body momentum distributions and other densities also show a dominance of np pairs [10, 12, 13, 17], in a agreement with results from exclusive experiments. Based on such calculations, it was also identified that the tensor force in the NN interaction is responsible for the np dominance [18].

Different approximated methods have been developed to describe the impact of short-range physics on different quantities. Some of these approaches assume a factorization of the ground-state wave function to a two-body function describing the correlated pair and a low-momentum function describing the remaining particles. This can be found already in the early works from the 1950's [2, 19, 20]. A universal description of correlated nucleons, neglecting the influence of the nuclear environment, was also suggested by Frankfurt and Strikman [21]. Ciofi degli Atti and Simula [22] have used a factorized form of the wave function to obtain a formula for the high-momentum tail of the spectral function, accounting for the contribution of deuteron-like pairs. Spectral function model was also developed by Benhar et al. [23], combining nuclear-matter calculations and the local density approximation to describe the impact of SRCs in finite nuclei, following the ideas of Ref. [24] for momentum distributions. Green's function methods were used by Dickhoff and others (see Ref. [25]). In addition, a method for calculating momentum distributions and other quantities was suggested by Ryckebusch et al., where the impact of short-range physics is implemented by the action of appropriate correlating operators on uncorrelated wave functions [26, 27]. Correlation functions were also introduced to account for the impact of SRCs on different quantities, including neutrinoless double beta decay matrix elements [28–32].

III. MODERN STUDIES OF SRCS

The nucleon SRCs in momentum space are rare high density fluctuations, representing correlations in the short space and time intervals. To resolve them one needs an external probe that can transfer a momentum significantly exceeding the relative momentum of nucleons in such short range correlations (SRCs). This emphasizes the importance of high energy scattering processes for the program of studies of short range nuclear structure. Historically, many successes in the exploration of short-distance phenomena (like QCD) are directly related to the studies of high energy and momentum transfer interaction of leptons with hadrons [33]. In extending this program to nuclear targets, the important question is what kind of strong interaction dynamics will be probed in high energy and momentum transfer scattering off the SRCs in nuclei?

The approach is that by varying the magnitudes of high energy- and momentum- transfer of the probe and using special kinematics to isolate high momentum component of nuclear wave function, we can probe the two- and three-nucleon systems at varying degrees of separations. We expect that, this approach will allow us eventually to reach the limit of hadronic degrees of freedom in nuclei, observing the onset of direct QCD dynamics.

A. Electron Scattering

1. *Inclusive electron scattering*

Inclusive (e,e') experiments are used to probe the abundance of SRC pairs in atomic nuclei. It was found that the cross-section ratio σ_A/A to σ_D/D between nucleus A and deuterium approaches a constant value that remains unaffected by the momentum and energy transfer in a kinematic regime which is sensitive to SRCs. This constant, referred to as a_2 value, provides an *estimate* of the relative abundance of neutron-proton (np) SRC pairs in nucleus A compared to deuterium [5]. The value of a_2 is sensitive to the center-of-mass motion of the pair, excitation of the residual nucleus, and potential contributions from 3N-SRCs.

The kinematic region necessary to access this scaling is characterized by $Q^2 \gtrsim 1.5$ GeV^2 and $1.5 \lesssim x_B \lesssim 1.9$. The lower bound of $x_B \sim 1.5$ implies that the nucleon's initial momentum must be comparable to the nuclear Fermi momentum, $k_F \sim 250$ MeV/c [5, 34–36]. The a_2 cross-section ratio has been extensively measured in the SRC scaling region across various experiments. Figure 1 shows a compilation of these measurements, and although there are some systematic discrepancies between different data sets, these do not appear to be substantial when considering the uncertainties involved, in which the ratio always takes the deuteron uncertainty.

Experimental results exhibited universal behavior, resulting in a nuclear cross-section ratio in the SRC-dominated region that is independent of both x_B and Q^2. Early studies suggested that the parameter a_2 would scale with the average nuclear density, approximated by $A^{-1/3}$. However, measurements from [37] demonstrated that ^{9}Be deviates significantly from this model, highlighting the importance of details of the nuclear structure. For heavier nuclei, the ratio remains approximately consistent, supporting the idea that the effect saturates in heavier nuclei. The cross-section ratio has also been measured using the mirror nuclei, tritium and helium, in the $x_B > 1$ region, as shown in Figure 2. The ratio in the SRC-dominated region is 0.854 ± 0.010 for $1.4 < x_B < 1.7$. Estimating the cross-section ratio for larger nuclei is a very complicated task, but the ratio for these light nuclei was well reproduced by the factorized cross-section approximation, which encapsulates all the many-body nuclear structure information in the spectral function. The spectral function used was extracted from exact calculations of the three-body ground state [38] using the AV18 interaction [39], without including irreducible three-body forces. The spectral function accounts for FSI between the two spectator nucleons but not with the leading nucleon.

2. *Proton knock out electron scattering measurements*

In proton knock out using high-energy electron scattering reactions $(e, e'p)$, where both the scattered electron and the knocked-out proton are detected, scaling behavior in the cross-section ratios of nuclei has been observed after selecting SRC kinematics with $Q^2 > 1.5$ GeV^2 and $250 < p_{\rm miss} < 600$ MeV/c [42], where $\vec{p}_{\rm miss} = \vec{p}_p - \vec{q}$ is the missing momentum of the knocked out nucleon. The observed scaling extends over a kinematic range of $0.7 \leq x_B \leq 1.8$, as shown in Fig. 3, much larger than in inclusive scattering due to the additional selectivity of the measured high-momentum pair nucleon. By examining the scaling onset in missing momentum, a universal transition in the scattering response is observed above the nuclear Fermi momentum. SRCs become dominant in nuclei at $p_{\rm miss} \sim 350$ MeV/c, well above the nuclear Fermi surface of $k_F \sim 250$ MeV/c.

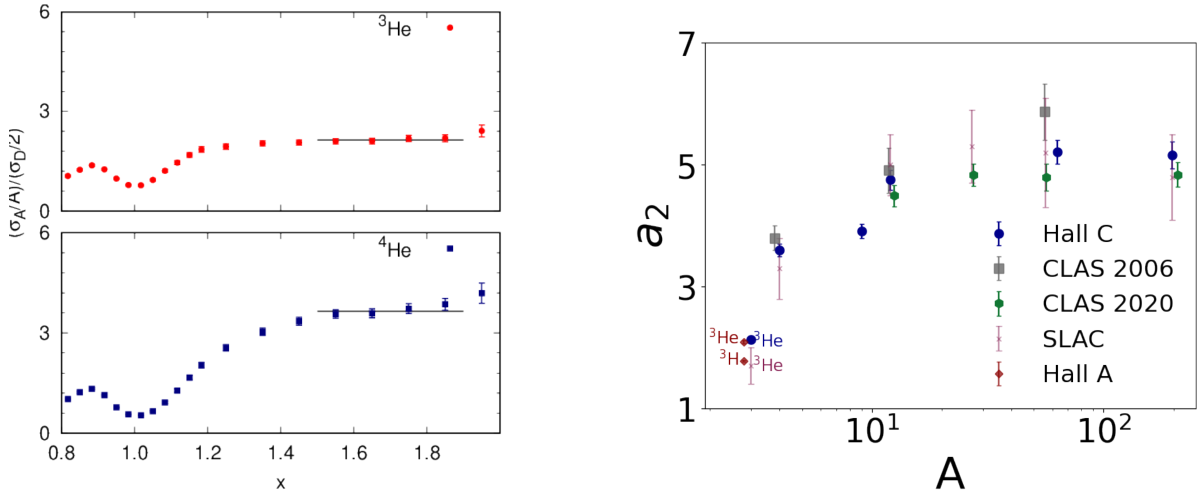

FIG. 1. Left: Inclusive cross section ratios for helium nuclei from E02-019 in Hall C [37]. Right: extracted values of a_2 vs A from measurements at SLAC [5], CLAS 2006 [34], Hall C [37] , CLAS 2020 [36] and Hall A [40].

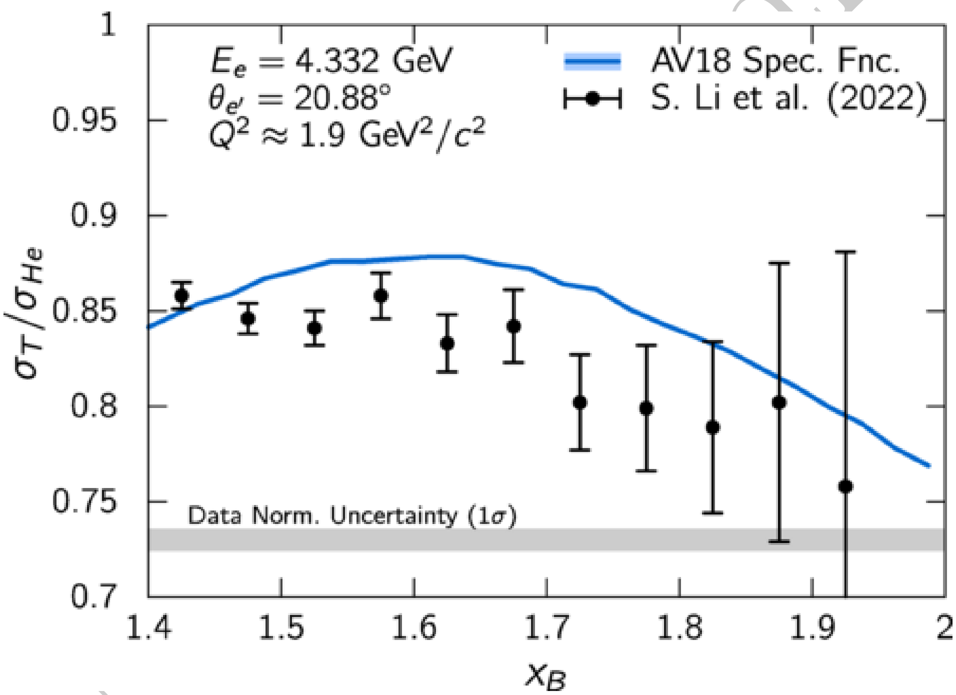

FIG. 2. Tritium to helium-3 (e, e') cross-section ratio, σ_T/σ_{He}, at $Q^2 \sim 1.9 GeV^2$ as a function of x$_B$. The experimental data, represented by black points, is taken from Ref. [40]. The theoretical prediction is derived from the factorized cross-section calculation, which employs an exact *ab initio* spectral function calculated using the AV18 interaction, as described by Ciofi [38]. The gray band shows the 1.18% data normalization uncertainty (1σ). Figure taken from [41].

Fig. 3 shows the extracted cross-section ratios per nucleon for carbon relative to deuterium as a function of x_B for different lower limits of p_{miss} in the left panel, and the integrated cross-section ratio over the range $0.7 \leq x_B \leq 1.8$ as function of pmiss in the right panel. The large-momentum dynamics of ^{12}C is in strong agreement with GCF calculations, which assume electron scattering from nucleons within SRC pairs, incorporating a realistic Gaussian center-of-mass momentum distribution [43]. The mean field region is well described by QMC calculations, while IPSM and Skyrme calculations are renormalized to match the experimental data at low missing momenta ($p_{miss} \leq 150$ MeV/c). This renormalization accounts for the depletion of single-nucleon strength resulting from long- and short-range correlations, as well as the influence of few-body reaction operators. This data also indicates that the transition from the mean-field to the SRC regime appears to occur at a missing momentum, p_{miss} of approximately 350–400 MeV/c.

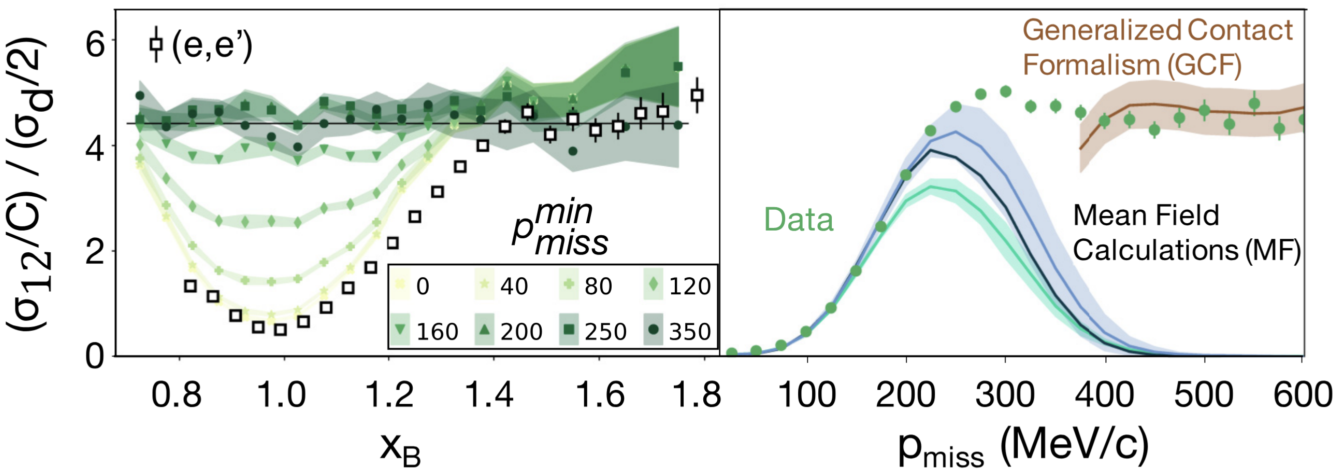

FIG. 3. Per-nucleon cross-section ratios for carbon relative to deuterium as a function of x_B (left panel) and p_{miss} (right panel). In the left panel, filled symbols in various colors correspond to different lower limits of the p_{miss} integration, with the upper limit fixed at 600 MeV/c. The colored bands represent the total uncertainty, encompassing both statistical and point-to-point systematic uncertainties, at the 68% confidence level. In the right panel, the cross-section ratios are integrated over the range $0.7 \leq x_B \leq 1.8$. The filled circles denote the experimental data. The brown line represents calculated cross sections for scattering off short-range correlated (SRC) nucleons in carbon, using the GCF model, while the other lines correspond to calculations for one-body mean-field nucleons, obtained from the QMC (teal), IPSM (black), and Skyrme (azure) models. Figure taken from [42].

3. *Two nucleon knockout Electron Scattering measurements*

Two nucleon knockout measurements were used to further probe SRCs pairs through a comprehensive data set from CLAS6 on a wide range of nuclei from ^{12}C to Pb [44–47]. The properties of SRC pairs are primarily studied from measurements of exclusive electron triple coincident hard breakup reactions. In these measurements, a nucleon in SRCs pairs is knocked out of the nucleus via a high momentum transfer reaction and detected in coincidence with the scattered electron and recoil nucleon balancing the high missing momentum p_{miss}. To ensure that the knockout proton originates from an SRC pair, selection cuts are applied including $Q^2 > 1.5$ (GeV/c)^2, $x_B > 1.1$ and $p_{miss} > 400$ MeV/c to also minimize contributions from FSI.

While the measured cross-section of $(e, e'p)$ is sensitive to the total number of both pp and np SRCs pairs in nuclei, the $(e, e'pp)$ measured cross-section is only sensitive to pp SRC pairs. The measurements showed that only a small fraction of $(e, e'p)$ events has a recoiling high missing momentum proton. This indicated that this proton-knockout reaction is dominated by np SRCs pairs. The first observables extracted from these data are cross-section double ratios for nuclei A relative to ^{12}C, $[A(e, e'pp)/A(e, e'p)]/[^{12}\text{C}(e, e'pp)/^{12}\text{C}(e, e'p)]$. This observable is not directly sensitive to the number of np SRCs pairs in nuclei, but it can be used to extract the ratio of np to the total number of SRC pairs in nuclei. The extracted fraction of np pairs showed that the dominance of np pairs is observed in all the nuclei measured from ^{12}C to ^{208}Pb by a factor of 20 [44].

The subsequent analysis was able to extract the triple coincidence $A(e, e'np)$ and $A(e, e'pp)$ as the first direct measurement of the pairs of SRC proton-proton (pp) and neutron-proton (np) SRCs pairs. The average reduced cross-section ratio pp to np is about 6% for all the nuclei measured from ^{12}C to Pb, see Fig.4. This result is consistent with previous measurements and supports the notion that np pair dominance in SRCs is a universal property from light to heavy nuclei [46]. This np dominance could be explained by the tensor force part of the nucleon-nucleon interaction within this momentum range. The tensor force only operates on spin-1 NN pairs. Because spin-1 pp pairs are suppressed by the Pauli exclusion principle, there are far more pn pairs than there are isospin-like SRC pairs. The results are consistent with calculations based on GCF framework using different NN interaction. This theoretical framework also is used to compared with measured $A(e, e'pp)/A(e, e'p)$ as a function of p_{miss}, see Fig.5. This ratio increases linearly from 400 to about 650 MeV/c and then appears to flatten out for all measured nuclei. This result

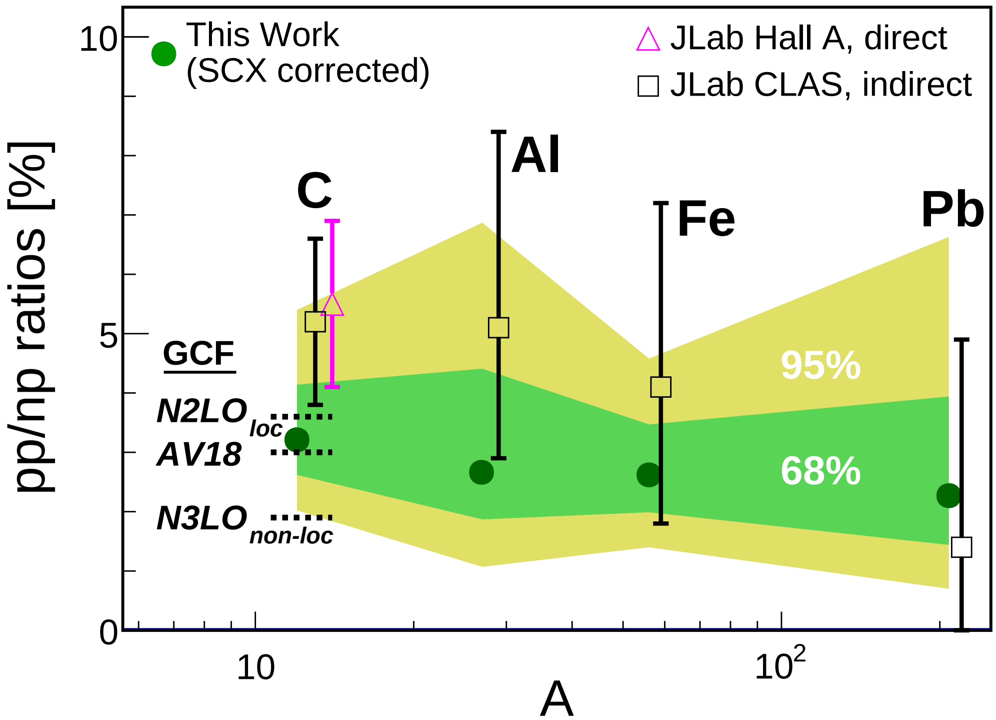

FIG. 4. Extracted ratio of pp to np pairs as function of atomic weight Acorrected for the single charge exchange (green filled circle), the shaded regions mark the 68% and 95% confidence level. Figure taken from[46]

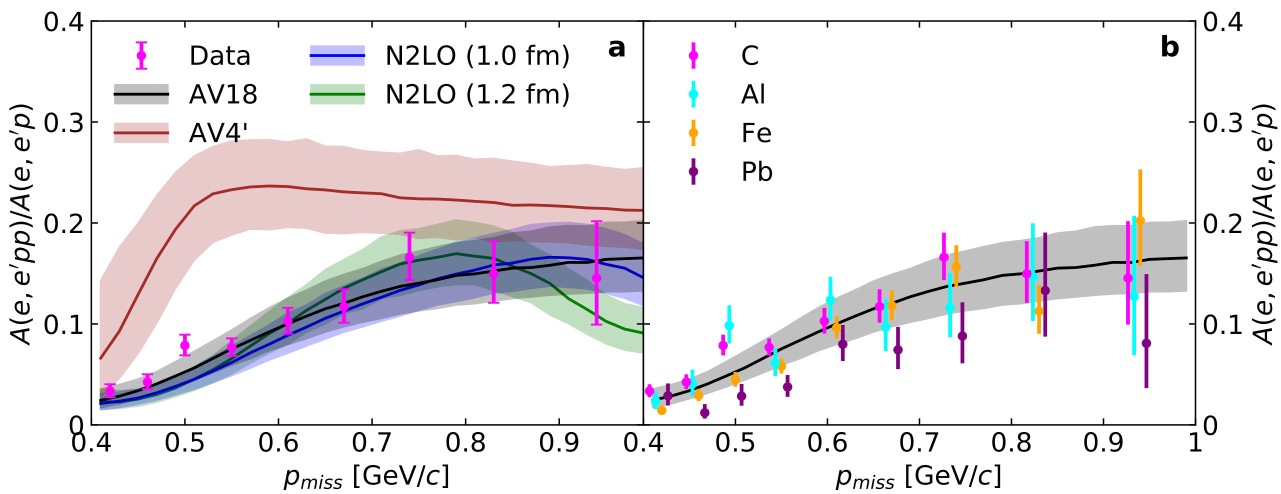

FIG. 5. Mesured ratio $A(e,e'pp)/A(e,e'p)$ as a function of p_{miss}. The left plot shows the ^{12}C results in comparison with GCF calculation using different NN interaction. The right plot shows results for multiple nuclei. The figure is taken from [47]

indicates the transition from a predominantly tensor interaction to a predominantly scale interaction at high p_{miss}.

The small center-of-mass (c.m.) motion is another fundamental characteristic of the SRCs pairs, crucial to understanding the SRC formation mechanism. This information was first extracted for ^{12}C using the measurement $A(p,2pn)$ [48] and later was extracted for ^{4}He and ^{12}C using $A(e,e'pp)$ and $A(e,e'pn)$ [49, 50]. The c.m. of the SRC pairs for heavier and asymmetric nuclei, aluminum, iron, and lead was extracted for the first time using $A(e,e'pp)$. This analysis showed that a three-dimensional Gaussian can describe the pair c.m. motion with a narrow width

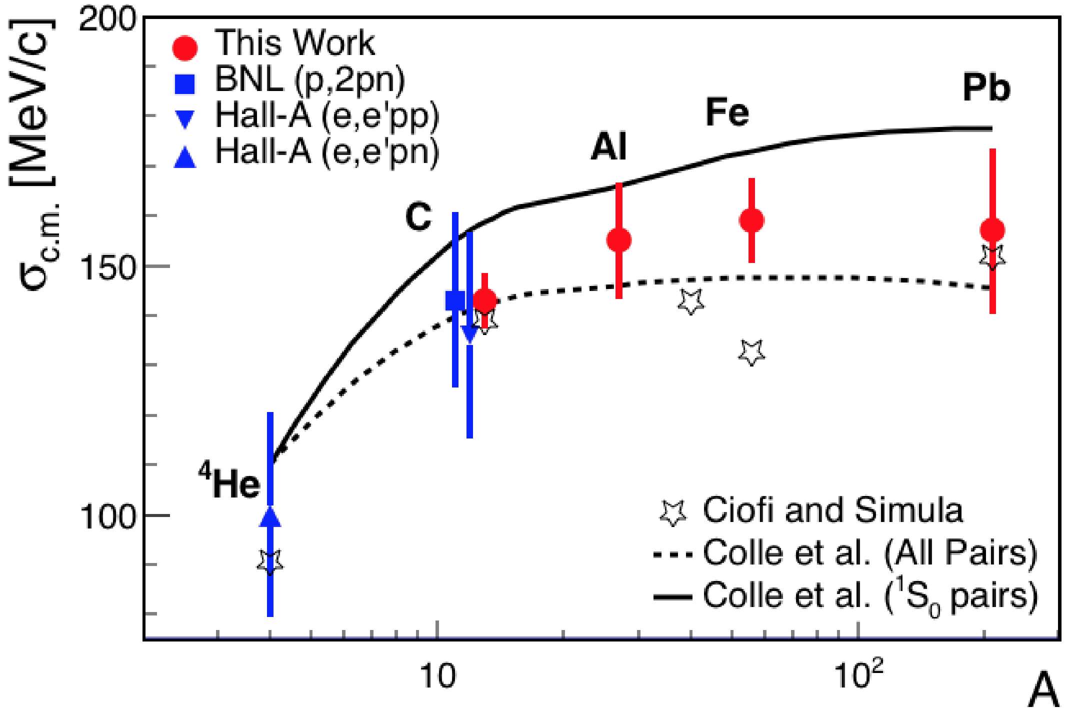

FIG. 6. The nuclear mass dependence of the one-dimentional width of the c.m. momentum distribution. the red data points are from $A(e,e'pp)$ measurements, compared with previous measurements (blue square and triangle), and with different theoretical calculations. Figure taken from [51]

Probe	Electron	Proton	Photon
Facilities	Halls A, B, C	BNL, JINR, GSI	Hall D
Cross section scaling (fixed Q^2, t)	s_{eN}^{0}	$\sim s_{pN}^{-10}$	$s_{\gamma N}^{-7}$

ranging from 140 to 170 MeV/c, approximately consistent with the sum of two mean-field nucleons with opposite momenta. The extraction of the width of the c.m. momentum distribution, $\sigma_{c.m.}$, for pp SRC pairs from $A(e,e'pp)$ for light to heavy nuclei combining multiple analysis can be seen in Fig. 6 [51]. The agreement in comparison with multiple theoretical calculations [52–54] supports that the SRCs pairs are formed from mean-field nucleons in specific quantum states [51].

Takeaways:

- Universal 2N scaling of inclusive cross section ratiosd
- Q^2 threshold for scaling observation
- All high momentum nucleon (above Fermi momentum) come in a pair
- SRC is np dominant and it is universal property due to the tensor force starting above Fermi momentum
- SRC pairs are back-to-back with smaller c.m compared to Fermi momentum

B. Hadronic probes

Electron-induced nucleon knockout reactions $(e,e'N)$ have been a successful and clean tool to probe nuclear ground-state distributions and SRCs for a few decades, as discussed in the previous sections. With similar sensitivity but different probe and underlying interaction, proton-induced $(p, 2p)$ knockout reactions have shown to be an important and complementary tool to study nuclear structure. Specifically, the quasi-elastic $(p, 2p)$ scattering at largest momentum transfer is a direct tool to probe single particle structure.

One example is the $^{12}\mathrm{C}(p, 2p)$ scattering at 90° center-of-mass scattering angle [55] that confirmed the validity of the quasi-elastic picture for probing ground-state momenta up to approximately $0.5\,\mathrm{GeV/c}$. The observed tail in the momentum distribution in that particular study is inconsistent with predictions of the independent particle model but aligns with the presence of a high-momentum tail above the Fermi sea, as was expected from two-nucleon short-range correlations [5, 55, 56]. This provided the first experimental evidence for probing SRCs in hadronic scattering, using data collected by the EVA spectrometer at the AGS accelerator at Brookhaven National Laboratory with proton-beam momenta of 5.9 and $7.5\,\mathrm{GeV/c}$.

Subsequently, multiple analysis employed these and additional datasets from triple-coincidence measurements $(p, 2p + n)$ as a novel approach to study NN short-range correlations [6, 57, 58]. These studies identified key signatures, including the back-to-back emission, low c. m. momentum, and the pre-dominance of np over pp pairs in $^{12}\mathrm{C}$ for the first time [6].

1. Proton knockout at large momentum transfer.

Similar to electron scattering, one method to probe SRC pairs with hadronic probes involved breaking the pair by scattering off one nucleon in the pair in a direct process, such as $(p, 2p)$ proton knockout, and measuring the struck nucleon, potentially along with the pair recoil nucleon.

To be sensitive to SRC high-momentum nucleons, early concepts and prior experiments have relied on reactions under large momentum transfer. Proton-beam knockout experiments conducted at momenta of $\sim 6\,\mathrm{GeV/c}$ and higher have achieved momentum transfers with magnitude $|t| > 5\,\mathrm{GeV^2/c^2}$. This large momentum transfer enhances resolving power, similar to electron scattering at high momentum transfer Q^2. Such conditions are in particular achieved with high energy beams and scattering angles around 90° c.m.

Furthermore, knockout measurements have validated the instantaneous approximation [55], describing the removal of a fast, bound proton through a hard reaction that can be described as a $pp \to pp$ sub-process [6]. Since multiple reaction mechanisms can lead to the same final state, it is critical to isolate the pair breakup in the nuclear ground state from initial and final state interactions.

The suppression of soft initial and final state interactions in these reactions supports the factorization of the hard pp scattering process from soft re-interactions. This factorization allows to express the cross section as the product of the pp scattering cross section off the bound proton and the nuclear decay function, enabling access to ground-state structure information [6].

2. Proton knockout in inverse kinematics.

Proton-beam experiments in normal kinematics benefit from relatively large cross sections and high-intensity beams. However, all common studies of SRCs in atomic nuclei, including electron scattering, face a significant limitation: these experiments typically cannot access or identify the final state of the $A-2$ system. This is because either the remnant is absorbed in the target material, or the missing energy resolution is insufficient to draw conclusions.

The $A-2$ system carries crucial information about the excitation energy of the spectator nucleus or the quantum numbers of its final state, making it a valuable source for understanding the reaction mechanism and SRC pair properties. To overcome this limitation, recent SRC experiments have adapted techniques from low-energy nuclear structure studies of radioactive ion beams performing experiments in so-called inverse and complete kinematics. In these experiments, the target nucleus itself is accelerated as a beam and studied in a reaction.

Such experiments are currently feasible only with proton probes, where high-energy ion beams ($\gtrsim 1\,\mathrm{GeV/u}$) scatter off a liquid hydrogen target. At these high beam energies, reaction products not directly involved in the reaction, particularly the $A-2$ system, move close to beam momentum. This allows their direct measurement, typically by using a magnetic spectrometer.

Pilot experiments have successfully demonstrated this approach at JINR with a stable $^{12}\mathrm{C}$ beam and at GSI-FAIR using $^{12}\mathrm{C}$ and $^{16}\mathrm{C}$ beams [59, 60]. Initial results are discussed below. The success of these studies in inverse kinematics opens new pathways to investigate SRCs not only in stable nuclei but also in asymmetric short-lived nuclei, extending the scope to nuclei far from the valley of β-stability, for example in a neutron-rich environment.

3. Recent results.

While the most detailed insights into SRC pair properties have traditionally come from electron scattering experiments, recent years have seen an increasing interest in using protons probes, focusing on studies in inverse kinematics.

A pioneering experiment – the first to measure SRC pair-breakup reactions in inverse kinematics – was performed at the Joint Institute for Nuclear Research (JINR) in Russia. Using a ^{12}C beam with a momentum of 4 GeV/c/u provided by the Nuclotron [59], the experiment probed np and pp pair breakup in the reaction $^{12}\mathrm{C}(p,2p)^{10}$B,Be. The modified BM@N setup allowed for coincident measurement of the struck pair and scattered target protons in coincidence with the heavy $A-2$ fragment.

The experiment first proved that through quasi-elastic proton knockout in $^{12}\mathrm{C}(p,2p)^{11}$B contributions from initial- and final-state interactions can effectively be separated by measuring the coincident fragment in inverse kinematics. This clear selection of quasi-free scattering conditions allows the reconstruction of the missing momentum and thus of the initial momentum of the struck nucleon in the boosted kinematics of $(p,2p)$ quasi-free scattering. For the bound $A-2$ system associated with the breakup of pn or pp pair, the experiment successfully confirmed, for the first time, sensitivity to SRCs in the nuclear ground state through kinematical selection in the $(p,2p)$ reaction and effective suppression of initial and final state interactions.

Despite limited statistics, identifying 23 pn and 2 pp pairs, the experiment confirmed key properties of SRC pairs, including np pair predominance [59]. By leveraging the $A-2$ fragment measurement, the experiment also achieved the first direct determination of the SRC pair c.m. momentum, under the assumption of scale separation for which the $A-2$ fragment momentum balances the SRC pair c.m. momentum. Additionally, the experiment provided first direct evidence for factorization between the $A-2$ system and the pair's relative momentum, demonstrating scale separation: the interaction of strongly correlated nucleons in the SRC high-momentum regime is unaffected by low-momentum nuclear physics.

Following the success of this pilot experiment that showed for the first time sensitivity to SRCs with hadronic probes in inverse kinematics, two additional experiments have been performed using this technique so far. A follow-up experiment at JINR aimed to boost statistics, while an experiment at GSI-FAIR investigates SRCs in the short-lived, neutron-rich nucleus ^{16}C [60].

The GSI-FAIR experiment, conducted at the R^{3}B setup with a beam momentum of approximately 2 GeV/c/u, seeks to explore SRC behavior in a neutron-rich system under controlled conditions. It also aims to probe SRCs at lower energies and momentum transfers, as current radioactive-ion beam facilities are limited to magnetic rigidities up to ~ 18 Tm. Both the JINR and GSI-FAIR datasets are currently under analysis, with results expected to provide further insights into SRC properties and extend the study of correlated nucleon pairs into new energy and isotopic regimes.

4. Probe independence and SRC g.s. distributions.

Modern studies of SRCs using hadronic probes concentrate on measurements in inverse kinematics. The first high-energy experiments employing SRC breakup reactions have demonstrated the ability to probe SRCs in the nuclear ground state. This is attributed to the effective suppression of contributions from initial- and final state interactions leveraging through coincident measurement of the $A-2$ fragment.

Data-simulation comparisons as shown in Ref. [59] and Fig. 7 show very good agreement, despite limited statistics. The experimental results support the back-to-back emission of the strongly correlated pair nucleons, while there is weak interaction between the pair relative momentum and the $A-2$ ^{10}B system, visible in an almost flat distribution The results strongly support the initial assumptions in the Generalized Contact Formalism, which serves as theoretical framework for interpreting the data. Although the interaction, reaction, and kinematics of hadronic probes differ significantly from those of electron or photon probes, the underlying physics seems to be consistent. This consistency suggests that hadronic probes can effectively access nuclear ground state distributions.

These promising results pave the way for an expanded experimental program, offering unique opportunities to deepen our understanding of SRC physics. The potential insights and directions for future research are discussed in Sec. V D.

Takeaways:

- hard proton scattering established as sensitive probe for SRC studies

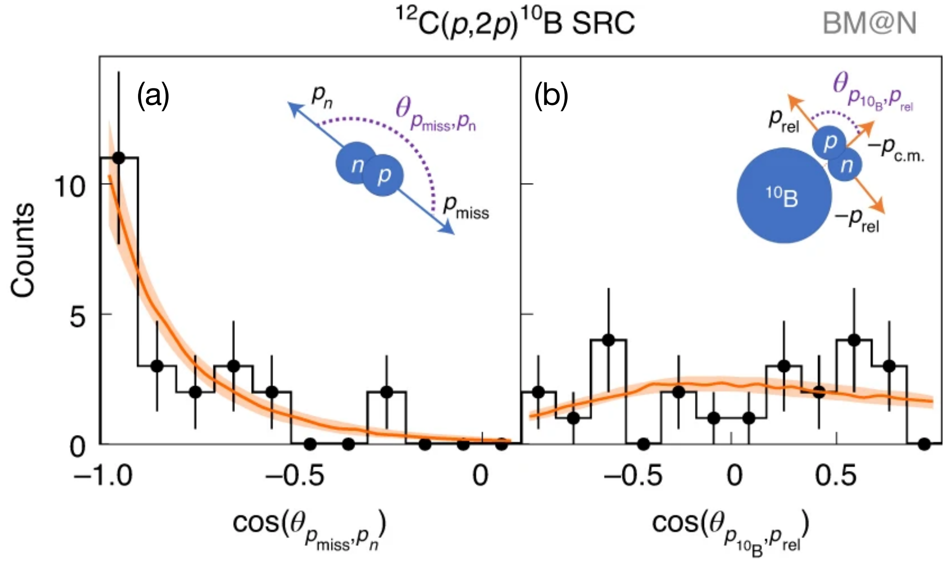

FIG. 7. Measured (black points) and GCF-simulated (orange line) $^{12}C(p, 2p)^{10}B$ events from JINR. (a) cosine of the angle between the recoil nucleon and missing momentum showing back-to-back emission. (b) angle between the ^{10}B fragment and pair relative momentum showing "weak" interaction, providing first direct indication for SRC-pair factorization. Figure taken from Ref. [59].

- inverse kinematics scattering opens unique and complementary paths to study SRC properties fully exclusively, particularly giving access to the $A-2$ system and unstable beams

- pilot experiments confirm np dominance and SRC pair kinematics, adding direct measurements of factorization and c. m. motion

C. Photon Probes

In addition to the quasi-elastic scattering measurements using electron and ion probes, the nuclear ground-state distributions have recently been probed through the use of real photon beams. Specifically, the use of "quasi-elastic meson photoproduction" $A(\gamma, mp)$ and $A(\gamma, mpp)$ consists of events where one or two nucleons are knocked out of the nucleus via the momentum-transfer from a meson photoproduction reaction ($\gamma N \to mp$), where m denotes the meson produced in the reaction. These reactions, when measured at large momentum-transfer $|t|$ and $|u|$, are capable of resolving the ground-state distributions of SRCs within the nucleus to provide a complement to previous measurements. As these reaction occur via different fundamental processes than electron- or hadron-scattering, they serve as an independent method of verifying a universal ground-state for SRCs. Photoproduction also offers unique access to initial-state neutrons via charge-exchange reactions $\gamma n \to m^- p$, which bypass the need for direct neutron detection, allowing for greater experimental access to neutrons within SRCs.

In addition to following different fundamental hard reactions as compared with electron- or hadron-scattering, quasi-elastic photoproduction experiences differences in a number of secondary reaction dynamics, including meson-exchange currents, isobar currents, and final-state interactions. Interpretation of electron-scattering data has been reliant on our ability to understand these effects, model their impact on observables, and isolate kinematics that minimize such deviations from plane-wave SRC breakup events. As the kinematics of photoproduction events differ significantly from electron-scattering (favoring perpendicular or parallel kinematics as compared with anti-parallel kinematics), the sensitivity of these events on non-plane-wave contributions differs in turn. Comparing the ground-state extracted using electron-, hadron-, and photon-scattering validates not only the reaction-universality of the extracted SRC properties, but also our ability to model and minimize these effects.

1. ρ Photoproduction as a Probe of SRCs

Two primary photoproduction channels are considered as the key probes of SRCs, these being the photoproduction of ρ^0 via the hard process $\gamma p \to \rho^0 p$ and the photoproduction of ρ^- via the hard process $\gamma n \to \rho^- p$.

The photoproduction of ρ^0 is promising due to the large cross section of this process; due to the phenomenon of "Vector Meson Dominance", the cross section for photoproduction of ρ^0 is considerably larger than that for any other meson, though the cross section drops rapidly with $|t|$. As a neutral meson channel, this scattering process can be treated analogously with electron- and proton- scattering measurements, with $(\gamma, \rho^0 p)$ and $(\gamma, \rho^0 pp)$ measurements giving access to SRC protons and proton-proton pairs, respectively, allowing for such measurements as $(\gamma, \rho^0 pp)/(\gamma, \rho^0 p)$ which give access to the isospin structure of SRCs as a function of relative momentum.

The photoproduction of ρ^- is useful for different reasons. While the cross section for ρ^- photoproduction is smaller than that for ρ^0, the hard process of $\gamma n \to \rho^- p$ gives unique experimental access to initial-state neutrons within the nucleus via final states consisting of charged particles and photons. As such, the measurements $(\gamma, \rho^- p)$ and $(\gamma, \rho^- pp)$ serve as a means of accessing SRC neutrons and neutron-proton pairs directly without the need for neutron detection, which is a unique advantage of photoproduction measurements.

SRC breakup events in these photoproduction reactions are identified by searching for events with large missing momentum, as in the case of semi-inclusive electron scattering. An equivalent to the electron-scattering scaling variable x_B can also be constructed with respect to the photoproduced meson, required to be large to minimize inelasticity in the reaction; for the same reason, the two-nucleon missing mass of the (γ, mp) reaction is required to be close to the nucleon mass to reduce contamination from events with missing particles. Finally, the momentum-transfer of the reaction $|t|$ and $|u|$ are required to be above ~ 1.5 GeV$^2/c^2$ to ensure resolution is sufficient for comparison to plane-wave predictions.

2. Hall D SRC/CT Experiment

The only experiment to date to perform a photonuclear probe of SRCs has been the Hall D SRC-CT Experiment [61] at Jefferson Lab. This experiment, performed in Fall 2021, used a tagged photon beam of energies $E_\gamma \sim 6 - 10.6$ GeV incident on deuterium, helium, and carbon targets. The large-acceptance GlueX spectrometer was used to measure the final-state charged particles and photons, enabling the detection of large multi-particle final-states necessary to resolve two-nucleon knockout with the photoproduction of a decaying meson.

Analysis of this experimental data is currently ongoing, with both of the above-described ρ^0 and ρ^- being examined as probes of SRC physics. Several analyses of this data have been completed[62, 63], most notably including a measurement of quasi-elastic photoproduction of J/ψ, which demonstrates the ability of these data to resolve missing-momentum quantities which are sensitive to internal nuclear structure. First results of SRC measurements from this data are expected to be available in the coming months. Initial analyses will focus on establishing the probe-dependence of extracted SRC properties by comparing these photoproduction results with previous electron- and proton-scattering measurement. Following analyses will aim to take advantage of the unique properties and kinematics of photoproduction. This includes the ability to precisely measure neutrons within SRC pairs via charge-exchange reactions, which no other experiment can easily access without challenging neutron detection. This will provide direct access to the abundant np-SRC pairs, which are typically indirectly measured.

Additionally, such access to initial-state neutrons may be essential to perform measurements of 3N-SRCs. Due to Fermi statistics, the vast majority of 3N-SRCs are expected to have compositions npp or nnp, containing at least one neutron; charge-exchange reactions $\gamma npp \to m^- ppp$ may thereby provide unique ability to probe such configurations with minimal background. It is yet unclear whether current photoproduction data has sufficient luminosity to access 3N-SRCs with sufficient statistics to claim a discovery.

Takeaways:

- High-energy photoproduction serves as independent probe of SRCs
- Charge-exchange reactions give unique access to initial-state neutrons within SRCs
- Data from first experiment being analyzed

IV. MODERN THEORY OF SRCS

A. High Energy Perspective

With the goal of probing a deeply bound nucleon in the nucleus with momentum comparable to its rest mass, the important issue are; (I) The description of *relativistic bound states* and (II) Self-consistent description of *hadron-quark transition in the nuclear wave function*. Both are outstanding issues and they are very important for the progress of understanding the QCD origin of nuclear forces at short distances. The high energy approach in addressing these issues is based on the factorization of SRC dynamics in nuclei that is probed by high energy scattering from the long range properties of nuclei. The approach is similar to the one that was used in *partonic* model of the nucleon. Similar to that the SRC state is described by Light-Front wave function and kinematic parameters are α_N and p_t - light-front momentum fraction of the SRC carried by the nucleon in the SRC and its transverse momentum (these are analogous to the LF momentum fraction of partons, x and its transverse momentum $k_\perp$ in the nucleon). The advantage of such description is that it clearly isolates SRC contribution and the observable which is light-front momentum distribution (similar to parton distribution function) can be extracted froodern inclusive high Q^2 measurements from nucleon at the SRC region.

1. *Problem of the Description of Relativistic Bound States and Inadequacy of Non Relativistic Quantum Mechanics*

Traditionally the theoretical approach in the description of quantum bound sates is rooted in non-relativistic (NR) Quantum Mechanics, in which bound state wave function is the solution of Schroedinger equation with the given potential and negative eigenvalue corresponding to the binding energy of the system. In this approach the wave function, for example, in the momentum space is normalized in such a way that probability density, integrated in the limits of (0, to ∞) is unity. It was quite a surprise that such a "normal" wave function resulted in a contradiction once applied to the calculation of scattering processes in relativistic domain. For example such a wave function violates the baryonic number and momentum sum rules (see e.g. [64–66]) and part of the wave function which contributes to the total normalization is kinematically forbidden for considered scattering processes.

In this case more natural approach is to relate the relativistic wave function normalization to the quantities that can be probed in the scattering process (such as nuclear electric charge or baryonic number) or quantities that are Lorentz boost invariant, such as the light-front momentum fraction carried by the constituents of the bound state.

The one illustration of the difference between non-relativistic quantum mechanical and high energy approaches is the deuteron: In non-relativistic Quantum Mechanics the deuteron is a bound state of the proton and neutron with positive parity, total angular momentum $J = 1$, and spin, $S = 1$. Using the non-relativistic relation that the parity of the state $P = (-1)^l$, one concludes that pn state has two internal angular momentum values $l = 0, 2$. Then the wave function of the deuteron is obtained by, first decomposing it into the radial, angular and spin components and then solving Schroedinger equation for the radial wave functions for the given pn potential.

However, in relativistic approach the deuteron is a composite pseudo-vector particle, for which the deuteron $\rightarrow$ proton-neutron transition can be expressed through the six invariant vertex functions from the most general principles. Then we investigate which of those vertex functions are leading and which are non-leading in high Q^2 limit.

In such formulation the question is, how to relate these transition vertices to the relativistic wave function of the nucleus. This can be achieved on the light-front (LF) in which case the scattering process can be expressed as LF-time, τ ordered diagrams (Fig.8). In these diagrams it can be shown that the quantity representing the ratio of phenomenological transition vertex $\Gamma^A_{N,(A-1)}$ to the light-front denominator of the propagating intermediate state (crossed by dashed vertical line, in Fig.8) is related to the light-front nuclear wave function of the interacting nucleon. It is important to emphasize that the light-front nuclear wave function of *massive* nucleons is not defined through the series of Fock-state decomposition of the nucleus but defined phenomenologically, in such a way that it represents the solution of the Weinberg type [67] equation for the bound states on the light-front (these equations in some way represent a projection of Bethe-Salpetter equations on the light-front). Additionally, in non-relativistic limit, the above defined light-front wave function reduces to NR wave function which is a solution of the Lippmann-Schwinger equation for the bound state. In such approach one does not construct the interaction potential on the light-front. Instead, once the analytic form of the LF wave function is established from general principles with given number of vertex functions we evaluate them based on modeling the interaction dynamics. In some way, the presented approach is similar to the calculation of electromagnetic current of the nucleon, in which case from general principles we introduce two, Dirac and Pauli form-factors and then work out to evaluate them through modeling and comparison with experiments on elastic eN scattering. One advantage in this case is that in NR limit the approach should reproduce results of non-relativistic nuclear physics, while no such limit exists for the case of nucleon form-factors.

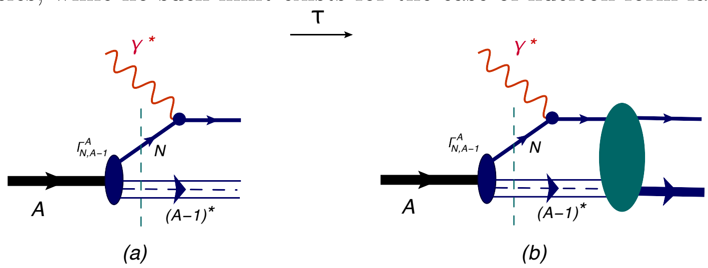

FIG. 8. Light-front time ordered diagram of scattering from the bound nucleon in the nucleus.

The presented approach has higher degree of reliability for the case of the deuteron, in which case the contributions from above mentioned six invariant vertices can be categorized as leading, first and second orders in the magnitude of small parameter, $\frac{k^2}{m_N\sqrt{Q2}}$, where k is the relative momentum of the pn system on the light front [68, 69]. This is an important simplification of high energy and momentum transfer scattering. In the center of mass of pn system two of the leading term vertices are related to the S- and D-states of the deuteron while the other is unknown, and has an extra factor of $\frac{k^2}{m_N^2}$ that indicates its pure relativistic nature. In practice we model the unknown vertex function and evaluate their parameters by comparing with experimental data.

The *uniqueness* of SRC studies is that due tow few-body character of correlations (2N or 3N) one can apply similar theoretical approach as used for the description of the deuteron to describe the SRC structure with relativistic internal momenta.

With the goal of probing a deeply bound nucleon in the nucleus with momentum comparable to its rest mass, the important issue is the description of the *relativistic bound system*. The other issue is the self-consistent description of *hadron-quark transition in the nuclear wave function*. Both are outstanding issues and they are very important for the progress of understanding the QCD origin of nuclear forces at short distances. The high energy methodology in addressing these issues is based on the factorization of SRC dynamics in nuclei that is probed by high energy scattering from the long range properties of nuclei. The approach is similar to the one that was used in partonic model of nucleon. Similar to that the SRC state is described by Light-Front wave function and kinematic parameters are α_N and p_t - light-front momentum fraction of the SRC carried by the nucleon in the SRC and its transverse momentum. The advantage of such description is that it clearly isolates SRC contribution and the observable which is light-front momentum distribution (similar to parton distribution function) can be extracted from inclusive high Q^2 measurements from nucleon at the SRC region.

2. *Incorporating QCD dynamics in electro-nuclear processes*

The above discussed approach provides also a consistent way for inclusion of quark-gluon degrees of freedom in nuclei. One example is the process in which the external probe scatters from a quark in the nucleus presented in Fig.9. Here again the scattering evolves along LF- time, τ, and calculational approach is based on the introduction of two transition vertices, first, $\Gamma^A_{N,A-1}$ - characterizing the process of resolving nucleon in the nucleus then the vertex $\Gamma^N_{q,R}$ characterizing the process of resolving quark in the nucleon leaving residual state, R. The part of the diagram identified as FSI is more complicated and can be modeled for specific reactions. Also, in the case in which closure approximation can be used the considered diagram will reproduce well known convolution model widely used in inclusive QCD processes involving nuclei.

The presented framework, however, allows to do more than reproduce convolution model, for example in the case of scattering from SRCs one can calculate the quark interchanges between two nucleons in the SRC. Also in the case of exclusive and (semi)-inclusive processes this approach allows to explore the dynamics of final state interaction that can include explicit quark-gluon degrees of freedom. Again as it was discussed in the previous section, it is important that scattering process is considered in high energy limit in which case significant simplifications can be achieved in the calculation.

For nuclear QCD, one complicated issue in our approach is that it requires modeling non-perturbative quark or gluon wave functions of nucleon. Similar to the discussion above this problem can be addressed in "positivist"

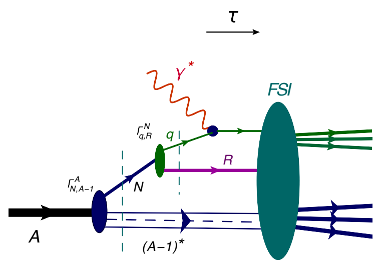

FIG. 9. Light-front time ordered diagram of external probe scattering from the quark in the nucleus.

approach, by introducing LF wave function of the object which is probed in the scattering process. The one issue that our approach addresses is the complication due to null-modes, for which the vacuum will not be trivial as it was expected previously[70]. In introducing LF quark wave function of the nucleon one does not expand it to the sum of Fock-components of massless quarks but consider the transition of nucleon to thee-valence quark + residual system, in which residual system presents the sum of all spectator quarks and gluons in the higher Fock-components as well as diagrams containing null mass $q\bar{q}$ systems. One models the wave function of the residual system and evaluate its parameters by comparing calculations with different deep-inelastic scattering data.

3. *Methodology of High Energy Approximations*

One of the main *methodologies* of the research is the effective light-front diagrammatic approach based on approximations that follow from high energy nature of the scattering process. The one challenge of strong interaction physics relevant to nuclear dynamics is the lack of the *small parameter* in the problem. What we found in our research is that high energy approximation allows to introduce a small parameter in the form of $\mid \frac{q_0-q_3}{q_0+q_3} \mid \ll 1$ where q_0 and q_3 are energy and momentum of virtual photon, both being significantly larger than the mass of the nucleon. It can be demonstrated [71] that in this limit reduction theorem can be proved which allows to sum potentially infinite number of nuclear scatterings into finite number of diagrams with effective/phenomenological vertices. In such approach the total nuclear scattering amplitude is expanded by the finite number ($\sim A$) of rescatterings. The approach is very tractable for lightest nuclei like deuteron and A=3 and in cases when higher order rescatterings are small it is applicable also for medium to large nuclei. The approach allows an inclusion of QCD degrees of freedom in a selfconsistent way which is essential for quantitative description of QCD effects in nuclear medium. With such a diagrammatic approach the electro-nuclear scattering process is calculated on the light-front allowing to deal with the relativistic kinematics for deeply bound nucleons. The approach is phenomenological since we do not expand nuclear or nucleon wave functions through the sum of mass-less Fock states of its constituents but model them using different approaches.

B. QMC methods

Quantum Monte Carlo (QMC) methods are ideally suited to study strongly correlated many-body systems, and allowing to correctly include hard nuclear interactions. However, they are limited to local nuclear potentials. Recently, their application has been extended to use chiral EFT Hamiltonians, thanks to the work carried out to derive local chiral EFT potentials, both with [72, 73] and without explicit delta degrees of freedom [74–76].

The many-body Hamiltonian which describes nucleons' interactions inside the nucleus can be written as

$$H = \sum_i T_i + \sum_{i<j} v_{ij} + \sum_{i<j<k} V_{ijk} + \dots \qquad (2)$$

where T_i is the one-body kinetic energy operator, v_{ij} is the nucleon-nucleon (NN) interaction, V_{ijk} is the three-nucleon (3N) interaction, and the ellipsis indicate interactions involving more than three particles. The indices i, j, and k run over the different nucleons. The NN interaction term generally comprises a long-range component, for inter-nucleon separation, due to one-pion exchange and intermediate- and short-range components. The AV18 interaction has been extensively and successfully used in a number of QMC calculations [39]. It can be written as an overall sum of 18 operators

$$v_{ij} = \sum_{p=1}^{18} v^p(r_{ij}) O_{ij}^p \tag{3}$$

Simplified versions of this interaction have been widely used, for instance the Argonne v_8' which contains a charge-independent eight operator projection, $O_{ij}^{p=1,8}$ but neglects terms describing charge and isospin symmetry breaking. In order to reproduce the correct binding for three body nuclei, the inclusion of 3N interactions is necessary. More specifically, two families of 3N interactions were obtained in combination with the AV18 potential: the Urbana IX (UIX) [77] and Illinois 7 (IL7) [78] models.

Despite their many successes, semi-phenomenological potentials exhibit several limitations. Notably, they fail to provide sufficient repulsion to ensure the stability of neutron stars when computing their equation of state. Additionally, they lack a rigorous framework for consistently deriving two- and many-body forces along with compatible electroweak currents. These shortcomings can be addressed by introducing chiral nuclear forces, which consist of both pion-exchange contributions and contact terms. The pion-exchange contributions govern the long-range part of nuclear interactions, while the contact terms encapsulate short-range physics. The strength of these contact terms is determined by unknown low-energy constants (LECs), which are constrained by fitting experimental data.

Similar to phenomenological interactions, the LECs governing the NN component are calibrated using NN scattering data up to 300 MeV laboratory energies, whereas those associated with three-nucleon forces are fixed by reproducing the properties of light nuclei. This optimization procedure involves a separate fit of the NN and 3N terms.

Variational Monte Carlo (VMC) is typically used to obtain a trial wave function, which serves as input for Green's Function Monte Carlo calculations. In VMC, the wave function is expressed as the product of long- and short-range correlation components:

$$|\Psi_T\rangle = \Big(1 - \sum_{i<j<k} F_{ijk}\Big)\Big(\mathcal{S}\prod_{i<j} F_{ij}\Big)|\Phi_j\rangle \tag{4}$$

where F_{ij} and F_{ijk} represent two- and three-body correlations, respectively. The symbol $\mathcal{S}$ denotes the symmetrization operator, while Φ_j represents the fully antisymmetric Jastrow wave function.

To find the optimal values of the parameters using a variational ansatz and minimizing the energy expectation value along with its associated variance with respect to the variational parameters:

$$E_T = \frac{\langle\Psi_T|H|\Psi_T\rangle}{\langle\Psi_T|\Psi_T\rangle} \geq E_0 \tag{5}$$

This evaluation is carried out using Metropolis Monte Carlo integration.

Given the optimal set of variational parameters, the trial wave function can be used as input for the GFMC calculation. This projects out the exact lowest-energy state Ψ_0 with the same quantum numbers:

$$|\Psi_0\rangle \propto \lim_{\tau\to\infty} e^{-(H-E_T)\tau}|\Psi_T\rangle\,. \tag{6}$$

In the above equation, τ is the imaginary time, and E_T is a parameter used to control the normalization. In addition to ground-state properties, excited states can be computed within GFMC. The direct computation of the propagator $e^{-H\tau}$ for arbitrary values of τ is typically not possible; instead, the integral above is evaluated for small imaginary times $\delta\tau = \tau/N$ with large N. More details can be found in Ref. [79].

The above imaginary-time propagation can also be used to extract dynamical properties of atomic nuclei. The energy dependence of the response functions can be inferred by computing their Laplace transform, dubbed as Euclidean response function [80]

$$\begin{aligned} E_\alpha(\mathbf{q},\tau) &= \int_{\omega_{\rm th}}^{\infty} d\omega\, e^{-\omega\tau} R_\alpha(\mathbf{q},\omega) \\ &= \langle\Psi_0|J_\alpha^\dagger(\mathbf{q}) e^{-(H-E_0)\tau} J_\alpha(\mathbf{q})|\Psi_0\rangle \qquad (7) \\ & \qquad (8) \end{aligned}$$

where the elastic contribution has to be subtracted as discussed in Ref. [81–83]. The calculation of the imaginary-time correlation operator is carried out with GFMC methods similar to those used in projecting out the exact ground state of H from a trial wave function a complete discussion of the methods is in Refs. [81–83].

Extracting the energy dependence of the response functions from their Euclidean counterparts is a nontrivial problem. For quasielastic responses which exhibit a smooth peak, a version of the maximum-entropy technique is used[81]. It has to be noted that machine-learning algorithms have recently been developed to invert the Laplace transform [84] and are capable of precisely reconstructing the low-energy transfer region of the response functions.

The GFMC, has already been extensively employed to perform *virtually exact* calculations of the electroweak response functions of ^{4}He and ^{12}C, retaining the full complexity of nuclear many-body correlations in both the initial and final states of the reaction [82, 83, 85]. Using interpolation procedures that rely on scaling ansatz, electron- and neutrino- scattering cross sections on these nuclear targets have been obtained [86, 87]. Furthermore, in Refs. [86, 88, 89] the relativistic effects in GFMC calculations of lepton–nucleus scattering are incorporated by choosing a reference frame that minimizes nucleon momenta.

QMC methods have been successfully employed to compute the one-nucleon spectral functions of nuclei up to ^{12}C. The spectral function encapsulates all the dynamical information of the nucleus and is defined for a nucleon with isospin $\tau_k = p, n$ and momentum $\mathbf{k}$ as

$$P_{\tau_k}(\mathbf{k}, E) = \sum_n |\langle \Psi_0 | [|k\rangle \otimes |\Psi_n^{A-1}\rangle]|^2 \delta(E + E_0 - E_n^{A-1}) . \tag{9}$$

Here, E denotes the excitation energy of the residual nucleus, $|k\rangle$ is the single-nucleon state, and $|\Psi_0\rangle$ is the nuclear ground state with energy E_0. The states $|\Psi_n^{A-1}\rangle$ and eigenvalues E_n^{A-1} correspond to the residual nucleus with $A-1$ nucleons.

The spectral function can be decomposed into a mean-field (MF) and a correlation term. The MF component accounts for shell structure, where nucleons occupy orbitals following the Pauli principle, predominantly contributing to low-momentum (k) and low-energy (E) regions. In contrast, the correlation term arises from nucleon pairs and triplets with low center-of-mass momentum but large relative momentum above the Fermi momentum k_F. Extensive experimental data from $(e, e'p)$ reactions indicate that short-range correlations deplete the single-nucleon strength in the MF region by approximately 20%, a feature largely independent of the nuclear system [42, 90–94].

Recently, QMC calculations have been used to determine the spectral functions for nuclei with $A = 3, 4,$ and 12. The MF contribution is computed from VMC spectroscopic overlaps between the nuclear ground state, a single-nucleon plane wave, and the bound states of the residual $A-1$ system. For medium-mass nuclei such as ^{12}C, multiple transitions involving both s- and p-shell nucleons must be considered. The correlation contribution is extracted using the two-nucleon momentum distribution $n_{\tau_k,\tau_{k'}}(\mathbf{k}, \mathbf{k}')$ from Ref. [95]. To isolate the effects of short-range correlations, cuts on the relative momentum of nucleon pairs are imposed, ensuring that both the normalization and shape of the one-nucleon momentum distributions are accurately reproduced.

In Ref. [89], the quantum Monte Carlo (QMC) spectral function (SF) of ^{12}C was employed to compute neutrino- and electron-scattering cross sections, incorporating both one- and two-body current operators. The results were compared with those obtained using the Green's function Monte Carlo (GFMC) method, and the impact of relativistic corrections was also analyzed.

Figure 10, adapted from Ref.[89], presents inclusive electron-^{12}C cross-section data for two distinct kinematics. For the SF calculations, both the QMC approach and the correlated basis function (CBF) method of Refs.[23, 96] were considered. The various curves represent different current contributions: the one-body current operator (1b), the interference between one- and two-body currents leading to one-nucleon emission (12b), and the two-body current resulting in two-nucleon emission (2b). Notably, in the 1b contribution, short-range correlations (SRCs) generate the characteristic tail in the high-energy transfer region.

The lower panels examine the role of relativistic effects in the GFMC calculations by comparing results in the laboratory (LAB) and active nucleon Breit (ANB) frames. The ANB frame incorporates relativistic effects, leading to observable differences. It is important to note that GFMC calculations currently cannot explicitly include pion degrees of freedom, which accounts for the suppressed strength in the large ω region.

For $A = 2$ and $A = 3$ nuclei, the spectral functions of these light nuclei have also been computed in Ref. [38] using the variational three-body wave function developed by the Pisa group for the AV18 potential to obtain the mean-field contribution to the spectral function. The background component was determined by solving the Schrödinger equation for the continuum using the same AV18 two-nucleon potential to derive the two-body wave function.

These spectral functions have been employed to describe $(e, e'p)$ scattering experiments on light nuclear targets in Refs. [100, 101]. To account for final-state interaction effects, a distorted spectral function is used, incorporating both the standard Glauber eikonal approximation and its generalized version.

Another approach that enables the calculation of electroweak response functions using quantum Monte Carlo (QMC) techniques is the Short-Time Approximation (STA). This method employs a factorization scheme that retains two-

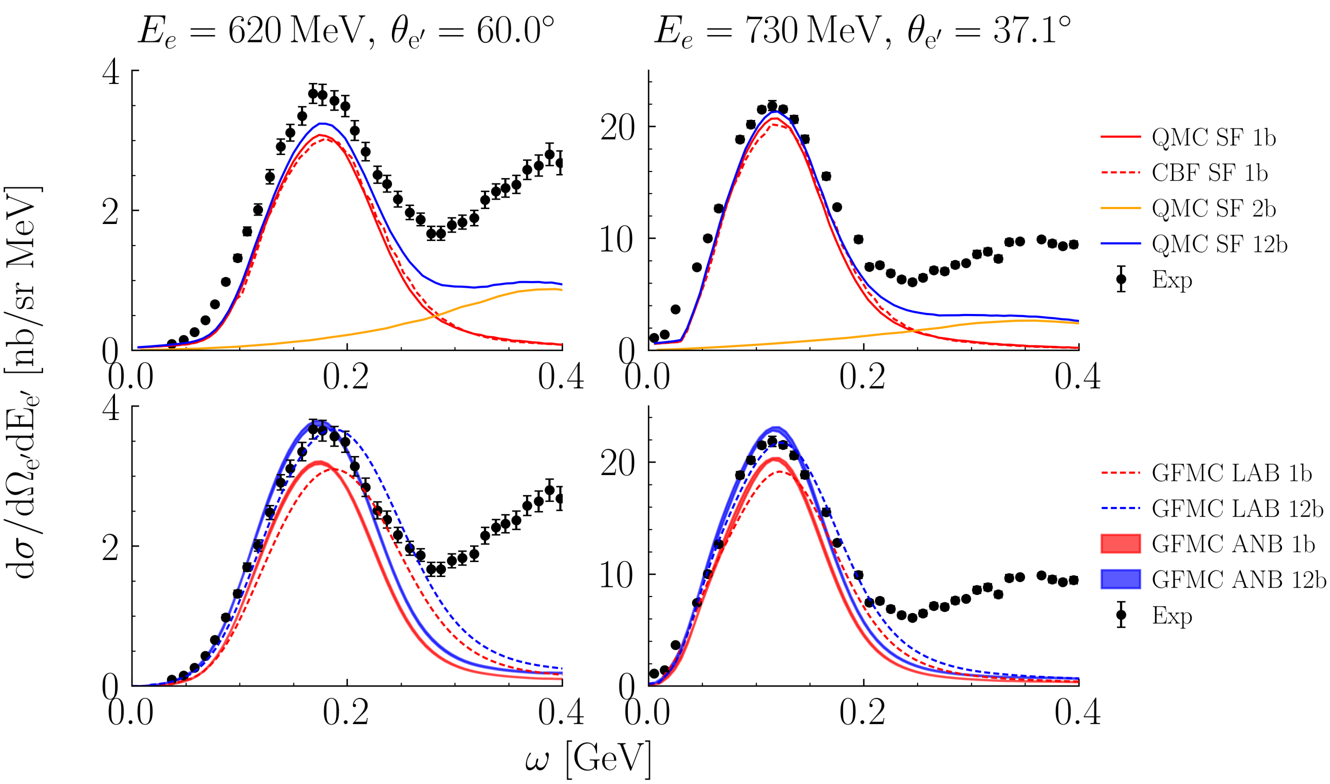

FIG. 10. Inclusive electron scattering comparisons at two different kinematics. Left: $E_{\mathrm{beam}} = 620\,\mathrm{MeV}$, $\theta_{e'} = 60°$. Right: $E_{\mathrm{beam}} = 730\,\mathrm{MeV}$, $\theta_{e'} = 37.1°$. Data is from Refs. [97–99]. Upper panels are for SF with QMC (CBF) one body in solid (dashed) red, QMC two-body in orange, and QMC one+two-body in blue. GFMC predictions are in the lower panel with dashed lines corresponding to response functions computed in the LAB frame, and solid for response functions in the ANB frame. Error bars on GFMC calculations include only errors from the inversion of the Euclidean response function, but neglect uncertainty due to interpolation of the responses.

body physics in both the currents and the strong interaction. The final states considered in this framework include only correlated nucleon pairs interacting with the external probe, leading to a significantly reduced computational cost compared to Green's Function Monte Carlo (GFMC) calculations, where the full A-nucleon system is propagated. While three-nucleon effects are not explicitly accounted for in the final state, the STA consistently incorporates interference terms between one- and two-nucleon currents, as well as two-nucleon correlations. Electromagnetic response functions and the corresponding cross sections for $A = 3$ nuclei have been presented and compared to GFMC and QMC spectral function (SF) calculations in Ref. [102], while results for $A = 12$ were recently reported in Ref. [103]. Unlike GFMC results, which are fully inclusive, the STA provides access to exclusive reactions, offering insights into the kinematics of the outgoing nucleon pair. Additionally, it can, in principle, accommodate explicit pion degrees of freedom.
Thus far, STA calculations have employed non-relativistic kinematics and currents. However, ongoing work aims to incorporate relativistic corrections in both aspects.

C. Generalized Contact Formalism

The generalized contact formalism (GCF) is an asymptotic theory that describes the short-range part of nuclear wave functions and the impact of short-range correlations on different nuclear quantities and observables.

This theory relies on the asymptotic factorization of the system into a strongly interacting pair and the remaining spectator nucleons, when two nucleons are found closed together in the nucleus. The correlated pair is described using a universal function, independent of the quantum state or the size of the nucleus. Contact parameters, obtained from the description of the spectator nucleons, provide the number of such correlated pairs in the specific system that is considered. The GCF is a generalization of the original contact theory, designed for atomic systems [], with significant

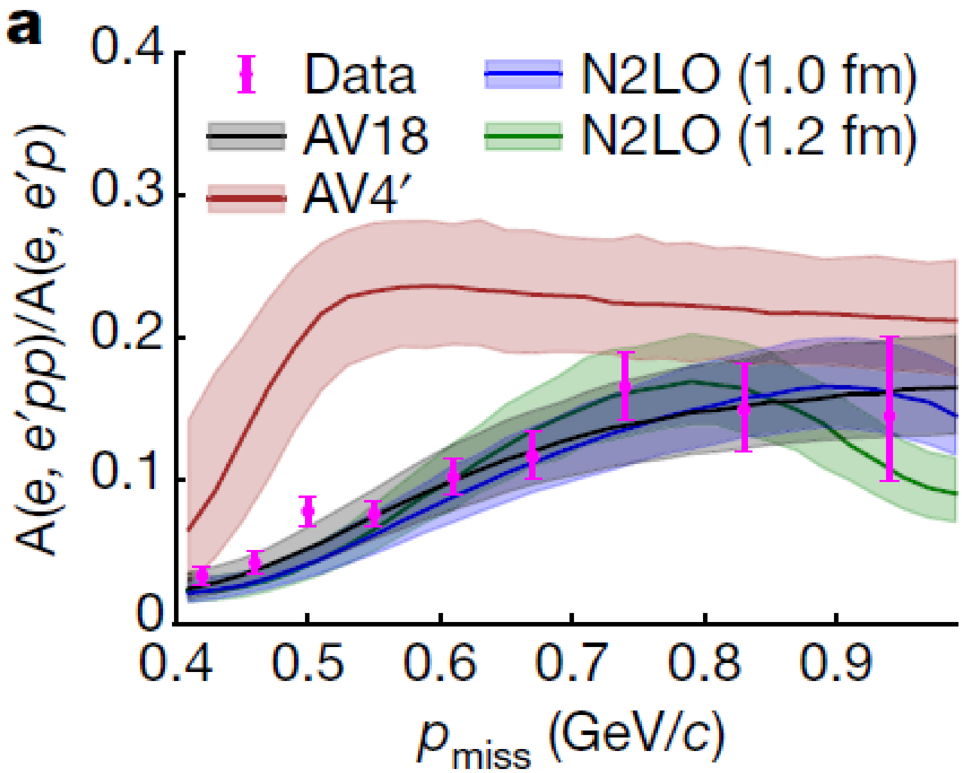

FIG. 11. Measured $(e, e'pp)/(e, e'p)$ event yield values as a function of the $(e, e'p)$ missing momentum for ^{12}C compared with theoretical calculations based on the GCF framework using different models of the NN interaction. All realistic models are in good agreement with the data. Figure taken from Ref. [104].

changes that had to be made to account for the complexity of the nuclear interaction. Eventually, matrices of contact parameters are defined, taking into account the different possible quantum numbers of SRC pairs.

One of the important aspects of the GCF is its ability to connect between *ab-initio* calculations and experimental data. Experimentally, nuclear SRCs are mainly studied using large-momentum-transfer electron scattering reactions, while *ab-initio* calculations are mostly limited to ground-state distributions or specific reactions and are unable to describe relevant experiments directly. The GCF describes both electron-scattering experimental data and nuclear distributions in the same framework, and, therefore, it bridges the gap between these two approaches and allows confronting them on a quantitative level, with direct connection to the underlying nuclear interaction models.

The GCF is used to derive the nuclear contact relations. These relations quantify the effects of SRC pairs on various nuclear quantities, such as momentum distributions, two-body densities, the spectral function, exclusive and inclusive electron-scattering cross sections, the Coulomb sum-rule and the photo-absorption cross section. All these quantities are related to the same parameters, the nuclear contacts, and therefore a network of relations among all these quantities is obtained.

Most of the nuclear contact relations were tested against experimental data or numerical calculations. Available *ab-initio* quantum Monte Carlo calculations were utilized to verify the short-range factorization of the many-body wave function and the GCF description of two-body densities at short distances and momentum distributions at high momenta. Exclusive electron-scattering data is also well described using the relevant GCF relations in a wide momentum and energy range, see Fig. 11 for an example.

The consistency of the different relations is also studied. A direct relation between the one-body and two-body momentum distributions, deduced from independent contact relations, is satisfied in *ab-initio* calculations. Similar agreement is seen for a direct connection between the photo-absorption cross section and momentum distributions, comparing *ab-initio* calculations with experimental data. Contact values extracted from either two-body momentum distributions or two-body densities are consistent with one another. The same contact values are also used in the successful description of the exclusive experimental data.

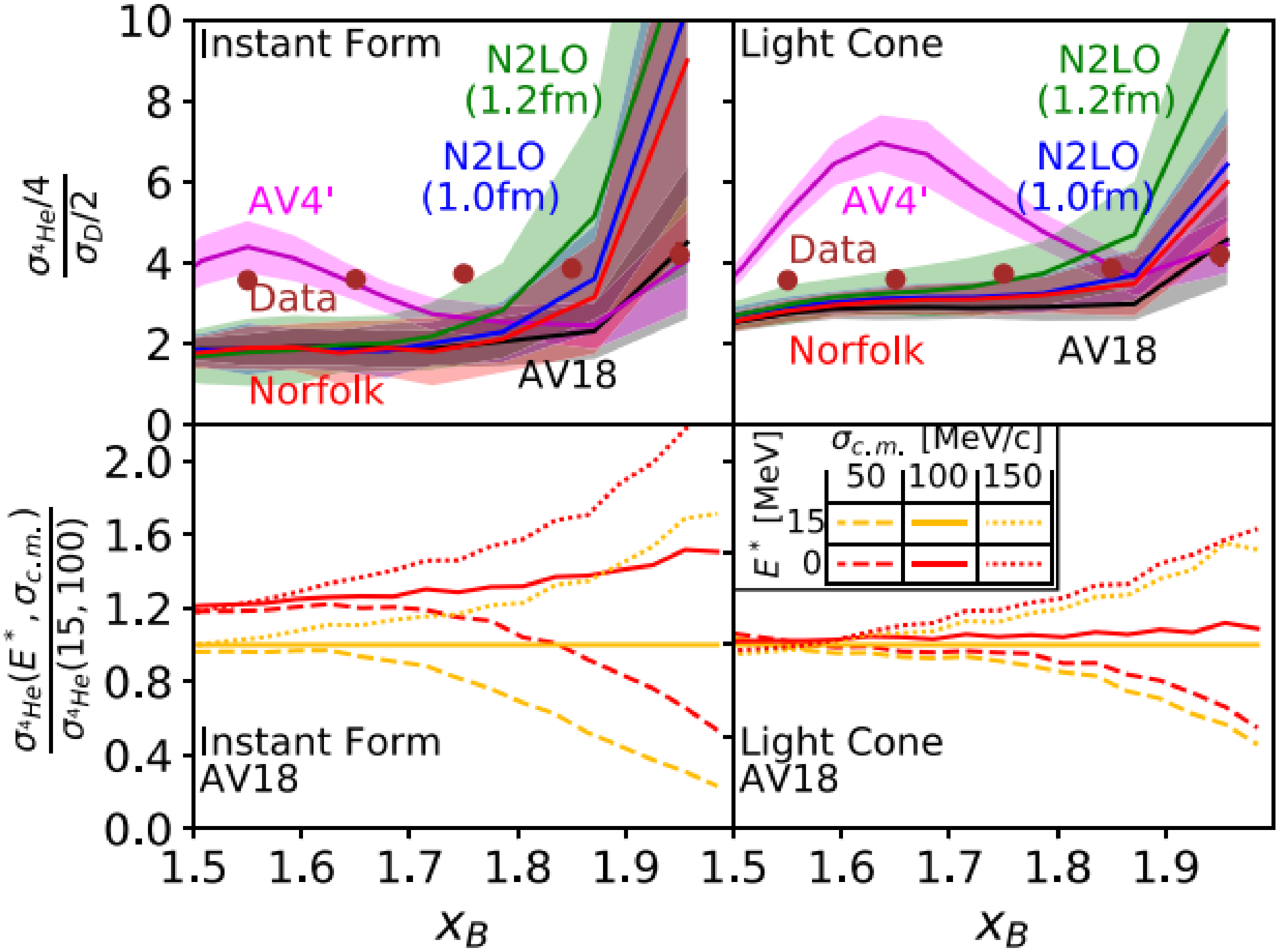

FIG. 12. Top: Measured per-nucleon inclusive cross-section ratios for ^{4}He over the deuteron as a function of x_B. The data [93] are compared with GCF calculations using both instant form (left) and light cone (right) formulations with different NN interaction models and using $\sigma_{c.m.} = 100 \pm 20$ MeV/c [43, 50], excitation energy $E^*_{A-2} = 0 - 30$ MeV, and contact parameters from Ref. [105]. The widths of the bands show their 68% confidence interval due to the uncertainties in the model parameters. Bottom: Ratio of the GCF calculated ^{4}He cross section with different excitation energies and c.m. momentum distribution widths to the cross section calculated for $E^*_{A-2} = 15$ MeV and $\sigma_{c.m.} = 100$ MeV/c. Calculations were done using both instant form (left) and light cone (right) GCF formulations with the AV18 NN interaction model. Figure taken from Ref. [106].

Currently, the only inconsistency is observed with regard to inclusive electron-scattering data. The GCF was used to study the traditional interpretation of the inclusive cross section as a measure for the abundance of SRC pairs in nuclei and it was found that it requires some important modifications. Nevertheless, there seems to be some inconsistency in the contact values needed to describe the inclusive data compared to the values obtained from *ab-initio* calculations. Accounting for relativistic effects using light-cone formulation seems to reduce some of the disagreement, see Fig. 12.

In addition, the GCF relations for the spectral function and the exclusive electron-scattering cross section allow simulating the relevant experiments. As a result, an improved analysis of the data can be performed using an event generator in which required corrections are applied in the simulation. This has led to more detailed and reliable comparison between theory and experimental data, and to new insights regarding SRC properties. The GCF is now an important tool used by experimental groups to analyze data and plan future experiments.

D. SRG approach

The Similarity Renormalization Group (SRG) approach casts SRC physics in an alternative low RG resolution picture. The renormalization group is a powerful tool that controls the resolution scale of the Hamiltonian, where the scale corresponds to the minimum wavelength or maximum momentum available for the wave functions of low-energy states of the Hamiltonian. This scale is not the same as the experimental resolution which is set by the momentum of the probe. At low RG resolution the Hamiltonian is "soft" in contrast to QMC and GCF approaches, meaning the ground-state wave function is amenable to mean-field approximations. The SRG in particular decouples low- and high-momentum scales with respect to the SRG resolution scale by applying unitary transformations to the Hamiltonian. SRC physics is shifted from nuclear structure to the reaction operators via unitary transformations without changing measured observables (e.g., cross sections).

In Ref. [4], key features of SRC phenomenology are reproduced within the SRG approach. Uncorrelated wave functions are described using simple ground-state wave functions with local density approximations, where SRG transformations shift the SRC physics into induced two-body operators. Analogous to the GCF factorization ansatz, SRG transformations factorize under a scale separation with respect to the SRG resolution scale [107, 108] matrix elements of high-momentum operators with low-momentum states factorize into a high-momentum piece independent of the nucleus and a nucleus-dependent low-momentum matrix element. This factorization explains the high-momentum universal tails of nucleon momentum distributions, where the dominant contribution comes from an SRG induced operator. Further applications of the SRG approach include deuteron electrodisintegration [More-2015, More-2017], the quasi-deuteron model [109], optical potentials [110], and matching low-RG resolution wave functions to high-resolution VMC momentum distributions [111].

V. GOING FORWARD

The observation of the dominance of the tensor component in 2N SRCs in nuclei indicates also that nuclear short range studies in the past decade succeeded in probing nuclear structure at distances down to $\sim 0.8 - 0.9$ fm with the *main conclusion* that the nucleonic component at such distances are still robust.

The next in the program is to extend the research to the domain of $k > 600$ MeV/c reaching to distances ($\sim 0.5 - 0.6$ fm), where one expects the dominance of the repulsion in the NN interaction. This will require a new generation of experiments at Jefferson Lab, taking advantage of 12 GeV high intensity continuous beam.

A. Current and New theory directions

B. Quantitative era of 2N-SRC

While great progress has been made in studies of 2N SRCs, there is still no full theoretical description of the data. (high statistic experiments, various nuclei, detailed momentum dependence, comparison to ab-initio calculations for light nuclei, improved models for heavier nuclei, relativistic effects, different probes, inverse kinematics...)

C. Discovery era of 3N-SRC

Correlations of three nucleons (3N-SRC) are also expected to exist, but have not yet been confirmed experimentally. Several attempts have been made with inclusive electron scattering, looking for a second scaling plateau in $A/^3He$ ratios. While the onset of 2N inclusive scaling plateau is well understood, the situation is less clear for 3N SRCs. Fig. 13 summarizes the searches with inclusive $A/^3He$ data so far. The Hall B data at $x > 2.2$ were shown to be an artifact of bin migration, so they do not actually probe the region of interest. The Hall A data show a consistent upward trajectory in the ratios at $x > 2$, whereas the Hall C data, taken at the highest Q^2, while suggestive of a plateau, have errorbars that prohibit a conclusive interpretation.

Recent theoretical work [112–115] suggests that 3N-SRCs do not begin to dominate until much higher Q^2 values than those of early searches, but the Hall C data [37] might be on the edge. Instead of looking at the onset of scaling in terms of x and Q^2, which are used to identify a minimum momentum of the struck nucleon in the target's rest frame, they use the light-cone variable α. This represents the light-cone nuclear momentum fraction carried by the struck nucleon, which more directly represents the nucleon momentum at large Q^2 values. For 3N-SRCs, one can define multiple versions of α_{3N} under different assumptions for the structure of the 3N-SRCs. Here, we take the convention of Ref. [113–115].

The model of Refs. [113–115] also makes a prediction for the probability of finding a nucleon in a 3N-SRC, $a_3(A)$, relative to 2N-SRCs, $a_2(A)$. Because 3N-SRCs come dominantly from two hard NN interactions, they find that $a_3(A) \propto a_2(A)^2$, assuming that 3N-SRCs are predominantly in *ppn* or *nnp* configurations. The authors of Ref [114, 115] go on to test this hypothesis by assuming scaling in this (α_{3N}=1.6 - 1.8) region for the E02-019 data and verifying that $a_3 \propto a_2^2$ for these data. This offers additional support that the E02-019 data were consistent with a 3N-SRC scaling plateau, but the result is again limited by the poor statistics of the ^{3}He data.

A recent work from E12-11-112 looked into the high-momentum components in ^{3}H and ^{3}He mirror nuclei through QE (e,e') scattering [40]. The A=3 systems have unique advantages in the search of new nuclear scaling due to 3N-SRCs. Because of the lower Fermi momentum in the A=3 nuclei, 2N-SRCs are expected to dominate the cross sections at smaller values of α. Consequently, the 3N-SRC configuration from two hard NN interaction would become dominant at smaller α_{3N}. Authors of Ref.[118] observed the onset of 2N-SRC scaling at $\alpha_{2N} \approx 1.2$ which corresponds to the initial nucleon momentum k >200 MeV/c. They then examined the ^{3}H/^{3}He cross sections at $\alpha_{3N} > 1.4$ ($k > 400$ MeV/c), and reported a ratio that is consistent with a 3N-SRC plateau with a height of $a_2(A=3)^2$.

This single data set with low α is not sufficient to establish the 3N-SRC scaling, but it provided more experimental options to search for 3N-SRC at intermediate Q^2 and higher statistics kinematics. Also, the A=3 studies provide clean picture of momentum-sharing and isospin structure of *nnp* and *npp* configurations, and also enable direct tests on our knowledge of 3N interaction theories at short distances

Thus, the question of 3N SRCs is still open and new, focused experimental searches are needed.

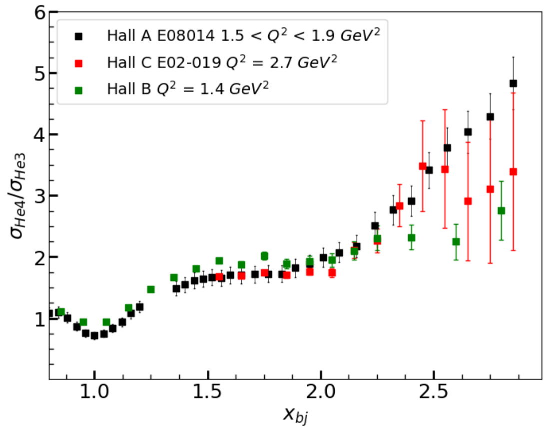

FIG. 13. Cross section ratios of $^4He/^3He$ from JLab experiments in Halls A,B, and C. [37, 116, 117]

D. Future using hadronic probes

The study of SRCs with hadronic probes is still in its early stages, with only three pioneering experiments performed in recent years. These experiments have laid the ground work, demonstrating that SRCs can successfully be probed in inverse kinematics with hadronic probes. This progress paves the way for developing a comprehensive research program that leverages conditions of inverse kinematics experiments, significant ones are laid out below. To advance this effort, theory developments in reaction theory and nuclear-structure theory are essential, in particular in the context of SRCs within the nuclear many-body system.

While electrons are the most incisive probe and it is essential to perform quantitative and detailed comparisons with high-statistics results from proton scattering, there are unique advantages associated with experiments in inverse kinematics using hadronic probes, which are discussed in the following and will define future research directions:

Inverse kinematics is the ability to access heavy fragments and recoils in boosted kinematics in coincidence, enabling a complete determination of the spectator system's final state that carries pair information. The $A-2$ excitation energy and quantum numbers are accessible through gamma-ray or invariant-mass spectroscopy. This can provide valuable insights into the ground state of the pair, such as its preferred quantum numbers [119–121], or the formation process [122]. The experiments conducted at JINR and GSI-FAIR have demonstrated the feasibility of this approach, but also highlighted the necessary improvements for the experimental setups in the future, including the need for large-acceptance and high-resolution detectors to for example boost statistics for precision or fully-exclusive experiments with multi-fragment detection. Furthermore, with suitable detection methods, a fully exclusive approach can contribute to the search for 3N SRCs by providing a "clean" identification of all SRC partners. Generally, studying SRCs in highly asymmetric nuclear systems, such as very neutron-rich short-lived nuclei, is only feasible in inverse kinematics. This approach opens the possibility for systematic studies, including studies along mass surfaces, with defined shell structure, and their interplay with nuclear many-body properties.

Hadronic probes remain an important tool for studying SRCs in nuclear ground states. The pilot experiments have focused on hard pair-breakup reactions at high energies, following a similar approach to electron scattering. However, most radioactive-ion beam facilities, such as FRIB (USA) and RIBF/RIKEN (Japan), can only provide secondary beams at few-hundred MeV/nucleon. Under these kinematic conditions, probing off-shell nucleons becomes difficult, so that alternative techniques are needed which have recently gained attraction. Among these techniques are nucleon pick-up reactions and deuteron knockout reactions. In such reactions, a proton probe picks up a high-momentum neutron from a pair to form a deuteron. The transferred momentum matches the initial momentum of the neutron in the pair, resulting in quasi-free deuteron scattering at forward angles [123]. This technique has previously been used to study the tensor interaction, as demonstrated in studies involving ^{16}O [123, 124]. In case of a deuteron knockout reaction, pre-formed deuterons are potentially sensitive to the SRC np pair abundance. The potential applicability of these reactions to radioactive-ion beams in inverse kinematics has inspired new proposals for experiments aimed at studying SRC np pairs.

It is worth noting that, while inverse kinematics offers unique advantages, proton scattering in normal kinematics, similar to electron scattering, provides a complementary approach. Such experiments allow at highest intensities to continue studies on probe independence, search for 3N SRCs, and non-nucleonic degrees of freedom and relativistic effects.

Focusing on the unique possibilities provided by fully-exclusive inverse-kinematics experiments with radioactive ion beams, only a few facilities currently have the capability to perform such experiments. These include GSI-FAIR to perform high-energy break-up reactions, and RIBF/RIKEN which has the potential to utilize pickup reactions at lower energies. The future FAIR facility (Germany) will be a flagship facility for high-energy RI beams. Similarly, the new HIAF facility (China) is expected to provide similar conditions, with experimental programs under development. The future upgrade of FRIB to 400 MeV/u primary beams could allow for studies similar to RIBF, but with current low beam energies, options remain limited. While these represent significant experimental developments, theory support is equally essential. This is includes advancing reaction theory, such as for deuteron knockout reactions, and conducting state-of-the-art nuclear structure calculation for light and medium-mass nuclei along isotopic chains.

Takeaways:

- benchmark results against electron probes
- perform quantitative experiments with increased statistics and acceptance in fully-exclusive kinematics
- unique inverse kinematics: spectroscopy of $A-2$ final state; radioactive-ion beams and systematic studies along isotopic chains
- explore alternative reaction kinematics (e. g. (p, pd))
- need for many-body calculations

[1] M. Preston and R. Bhaduri, *Structure of the Nucleus* (Addison-Wesley, 1975).
[2] K. A. Brueckner, R. J. Eden, and N. C. Francis, High-Energy Reactions and the Evidence for Correlations in the Nuclear Ground-State Wave Function, Phys. Rev. **98**, 1445 (1955).
[3] R. J. Furnstahl and A. Schwenk, How should one formulate, extract, and interpret 'non-observables' for nuclei?, J. Phys. G **37**, 064005 (2010), arXiv:1001.0328 [nucl-th].
[4] A. J. Tropiano, S. K. Bogner, and R. J. Furnstahl, Short-range correlation physics at low renormalization group resolution, Phys. Rev. C **104**, 034311 (2021), arXiv:2105.13936 [nucl-th].
[5] L. L. Frankfurt, M. I. Strikman, D. B. Day, and M. Sargsian, Evidence for short range correlations from high Q**2 (e, e-prime) reactions, Phys. Rev. C **48**, 2451 (1993).
[6] E. Piasetzky, M. Sargsian, L. Frankfurt, M. Strikman, and J. W. Watson, Evidence for the strong dominance of proton-neutron correlations in nuclei, Phys. Rev. Lett. **97**, 162504 (2006), arXiv:nucl-th/0604012.
[7] R. Subedi *et al.*, Probing Cold Dense Nuclear Matter, Science **320**, 1476 (2008), arXiv:0908.1514 [nucl-ex].
[8] H. Feldmeier, W. Horiuchi, T. Neff, and Y. Suzuki, Universality of short-range nucleon-nucleon correlations, Phys. Rev. C **84**, 054003 (2011), arXiv:1107.4956 [nucl-th].
[9] M. Alvioli, C. Ciofi degli Atti, L. P. Kaptari, C. B. Mezzetti, and H. Morita, Nucleon momentum distributions, their spin-isospin dependence and short-range correlations, Phys. Rev. **C87**, 034603 (2013), arXiv:1211.0134 [nucl-th].
[10] R. B. Wiringa, R. Schiavilla, S. C. Pieper, and J. Carlson, Nucleon and nucleon-pair momentum distributions in $a \leq 12$, Phys. Rev. C **89**, 024305 (2014).
[11] A. Rios, A. Polls, and W. H. Dickhoff, Density and isospin asymmetry dependence of high-momentum components, Phys. Rev. **C89**, 044303 (2014), arXiv:1312.7307 [nucl-th].
[12] L. E. Marcucci, F. Sammarruca, M. Viviani, and R. Machleidt, Momentum distributions and short-range correlations in the deuteron and ^{3}He with modern chiral potentials, Phys. Rev. C **99**, 034003 (2019), arXiv:1809.01849 [nucl-th].
[13] M. Piarulli, S. Pastore, R. B. Wiringa, S. Brusilow, and R. Lim, Densities and momentum distributions in A≤12 nuclei from chiral effective field theory interactions, Phys. Rev. C **107**, 014314 (2023), arXiv:2210.02421 [nucl-th].
[14] M. Alvioli, C. Ciofi degli Atti, and H. Morita, Ground-state energies, densities and momentum distributions in closed-shell nuclei calculated within a cluster expansion approach and realistic interactions, Phys. Rev. C **72**, 054310 (2005), arXiv:nucl-th/0506054.
[15] M. Alvioli, C. Ciofi Degli Atti, L. P. Kaptari, C. B. Mezzetti, and H. Morita, Universality of nucleon-nucleon short-range correlations and nucleon momentum distributions, Int. J. Mod. Phys. **E22**, 1330021 (2013), arXiv:1306.6235 [nucl-th].
[16] J. Lynn, D. Lonardoni, J. Carlson, J. Chen, W. Detmold, S. Gandolfi, and A. Schwenk, Ab initio short-range-correlation scaling factors from light to medium-mass nuclei, J. Phys. G **47**, 045109 (2020), arXiv:1903.12587 [nucl-th].
[17] T. Neff, H. Feldmeier, and W. Horiuchi, Short-range correlations in nuclei with similarity renormalization group transformations, Phys. Rev. C **92**, 024003 (2015).
[18] M. Alvioli, C. Ciofi degli Atti, and H. Morita, Proton-neutron and proton-proton correlations in medium-weight nuclei and the role of the tensor force, Phys. Rev. Lett. **100**, 162503 (2008).

[19] J. S. Levinger, The High-energy nuclear photoeffect, Phys. Rev. **84**, 43 (1951).

[20] J. Heidmann, The Production of High Energy Deuterons by Energetic Nucleons Bombarding Nuclei, Phys. Rev. **80**, 171 (1950).

[21] L. Frankfurt and M. Strikman, Hard nuclear processes and microscopic nuclear structure, Phys. Rep. **160**, 235 (1988).

[22] C. Ciofi degli Atti and S. Simula, Realistic model of the nucleon spectral function in few- and many-nucleon systems, Phys. Rev. C **53**, 1689 (1996).

[23] O. Benhar, A. Fabrocini, S. Fantoni, and I. Sick, Spectral function of finite nuclei and scattering of GeV electrons, Nucl. Phys. A **579**, 493 (1994).

[24] S. Stringari, M. Traini, and O. Bohigas, Momentum distribution in heavy nuclei, Nucl. Phys. A **516**, 33 (1990).

[25] W. H. Dickhoff and C. Barbieri, Selfconsistent Green's function method for nuclei and nuclear matter, Prog. Part. Nucl. Phys. **52**, 377 (2004), arXiv:nucl-th/0402034.

[26] J. Ryckebusch, M. Vanhalst, and W. Cosyn, Stylized features of single-nucleon momentum distributions, Journal of Physics G: Nuclear and Particle Physics **42**, 055104 (2015).

[27] J. Ryckebusch, W. Cosyn, T. Vieijra, and C. Casert, Isospin composition of the high-momentum fluctuations in nuclei from asymptotic momentum distributions, Phys. Rev. C **100**, 054620 (2019), arXiv:1907.07259 [nucl-th].

[28] G. A. Miller and J. E. Spencer, A Survey of Pion Charge-Exchange Reactions with Nuclei, Annals Phys. **100**, 562 (1976).

[29] F. Simkovic, A. Faessler, H. Muther, V. Rodin, and M. Stauf, The 0 nu bb-decay nuclear matrix elements with self-consistent short-range correlations, Phys. Rev. **C79**, 055501 (2009), arXiv:0902.0331 [nucl-th].

[30] R. Roth, H. Hergert, P. Papakonstantinou, T. Neff, and H. Feldmeier, Matrix elements and few-body calculations within the unitary correlation operator method, Phys. Rev. C **72**, 034002 (2005), arXiv:nucl-th/0505080.

[31] O. Benhar, R. Biondi, and E. Speranza, Short-range correlation effects on the nuclear matrix element of neutrinoless double-Î$^{\mathbf{2}}$ decay, Phys. Rev. **C90**, 065504 (2014), arXiv:1401.2030 [nucl-th].

[32] R. Cruz-Torres, A. Schmidt, G. A. Miller, L. B. Weinstein, N. Barnea, R. Weiss, E. Piasetzky, and O. Hen, Short range correlations and the isospin dependence of nuclear correlation functions, Phys. Lett. **B785**, 304 (2018), arXiv:1710.07966 [nucl-th].

[33] R. P. Feynman, *Photon-Hadron Interactions* (CRC Press, 1972).

[34] K. Egiyan *et al.* (CLAS Collaboration), Measurement of 2- and 3-nucleon short range correlation probabilities in nuclei, Phys. Rev. Lett. **96**, 082501 (2006).

[35] N. Fomin *et al.*, New measurements of high-momentum nucleons and short-range structures in nuclei, Phys. Rev. Lett. **108**, 092502 (2012).

[36] B. Schmookler *et al.* (CLAS Collaboration), Modified structure of protons and neutrons in correlated pairs, Nature **566**, 354 (2019).

[37] N. Fomin *et al.*, New measurements of high-momentum nucleons and short-range structures in nuclei, Phys. Rev. Lett. **108**, 092502 (2012).

[38] C. Ciofi degli Atti and L. P. Kaptari, Calculations of the exclusive processes H-2(e, e-prime p)n, He-3(e, e-prime p)H-2 and He-3(e, e-prime p)(pn) within a generalized Glauber approach, Phys. Rev. C **71**, 024005 (2005), arXiv:nucl-th/0407024.

[39] R. B. Wiringa, V. G. J. Stoks, and R. Schiavilla, An Accurate nucleon-nucleon potential with charge independence breaking, Phys. Rev. C **51**, 38 (1995), arXiv:nucl-th/9408016.

[40] S. Li *et al.*, Revealing the short-range structure of the mirror nuclei ^{3}H and ^{3}He, Nature **609**, 41 (2022).

[41] A. Schmidt *et al.*, A=3(e,e')xB≥1 cross-section ratios and the isospin structure of short-range correlations, Phys. Rev. C **109**, 054001 (2024), arXiv:2402.08199 [nucl-th].

[42] I. Korover *et al.* (CLAS), Observation of large missing-momentum (e,e'p) cross-section scaling and the onset of correlated-pair dominance in nuclei, Phys. Rev. C **107**, L061301 (2023), arXiv:2209.01492 [nucl-ex].

[43] E. O. Cohen *et al.* (CLAS Collaboration), Center of Mass Motion of Short-Range Correlated Nucleon Pairs studied via the $A(e, e'pp)$ Reaction, Phys. Rev. Lett. **121**, 092501 (2018), arXiv:1805.01981 [nucl-ex].

[44] O. Hen *et al.*, Momentum sharing in imbalanced Fermi systems, Science **346**, 614 (2014), arXiv:1412.0138 [nucl-ex].

[45] M. Duer *et al.* (CLAS Collaboration), Probing high-momentum protons and neutrons in neutron-rich nuclei, Nature **560**, 617 (2018).

[46] M. Duer *et al.* (CLAS Collaboration), Direct Observation of Proton-Neutron Short-Range Correlation Dominance in Heavy Nuclei, Phys. Rev. Lett. **122**, 172502 (2019), arXiv:1810.05343 [nucl-ex].

[47] A. Schmidt *et al.* (CLAS), Probing the core of the strong nuclear interaction, Nature **578**, 540 (2020), arXiv:2004.11221 [nucl-ex].

[48] A. Tang *et al.*, n-p short range correlations from (p,2p + n) measurements, Phys. Rev. Lett. **90**, 042301 (2003), arXiv:nucl-ex/0206003.

[49] R. Shneor *et al.* (Jefferson Lab Hall A), Investigation of proton-proton short-range correlations via the C-12(e, e-prime pp) reaction, Phys. Rev. Lett. **99**, 072501 (2007), arXiv:nucl-ex/0703023.

[50] I. Korover, N. Muangma, O. Hen, *et al.*, Probing the Repulsive Core of the Nucleon-Nucleon Interaction via the 4He(e,e'pN) Triple-Coincidence Reaction, Phys. Rev. Lett. **113**, 022501 (2014).

[51] E. Cohen, M. Duer, E. Piasetzky, O. Hen, and L. Weinstein, Extracting the center-of-mass momentum distribution of *pp*-SRC pairs in ^{12}C, ^{27}Al, ^{56}Fe, and ^{208}Pb, CLAS EG2 Analysis Note (2018).

[52] C. Ciofi degli Atti and S. Simula, Realistic model of the nucleon spectral function in few and many nucleon systems, Phys. Rev. C **53**, 1689 (1996).

[53] M. Vanhalst, J. Ryckebusch, and W. Cosyn, Quantifying short-range correlations in nuclei, Phys. Rev. C **86**, 044619

(2012).

[54] C. Colle, W. Cosyn, J. Ryckebusch, and M. Vanhalst, Factorization of exclusive electron-induced two-nucleon knockout, Phys. Rev. **C89**, 024603 (2014).

[55] Y. Mardor *et al.*, Measurement of quasielastic C-12 (p, 2p) scattering at high momentum transfer, Phys. Lett. B **437**, 257 (1998), arXiv:nucl-ex/9710002.

[56] L. L. Frankfurt and M. I. Strikman, Hard Nuclear Processes and Microscopic Nuclear Structure, Phys. Rept. **160**, 235 (1988).

[57] J. Aclander *et al.*, The large momentum transfer reaction C-12(p,2p + n) as a new method for measuring short range N N correlations in nuclei, Phys. Lett. B **453**, 211 (1999).

[58] A. Tang *et al.*, n-p short range correlations from (p,2p + n) measurements, Phys. Rev. Lett. **90**, 042301 (2003), arXiv:nucl-ex/0206003.

[59] M. Patsyuk *et al.* (BM@N), Unperturbed inverse kinematics nucleon knockout measurements with a 48 GeV/c carbon beam, Nature Physics **17**, 693 (2021), arXiv:2102.02626 [nucl-ex].

[60] The R^3B Collaboration, Proposal S522: First characterization of Short-Range Correlations in exotic nuclei at R^3B (non-public).

[61] O. Hen *et al.*, Studying short-range correlations with real photon beams at gluex (2020), arXiv:2009.09617 [nucl-ex].

[62] J. Pybus *et al.*, Search for axion-like particles through nuclear primakoff production using the gluex detector, Physics Letters B **855**, 138790 (2024).

[63] J. R. Pybus *et al.*, First measurement of near- and sub-threshold j/ψ photoproduction off nuclei (2024), arXiv:2409.18463 [nucl-ex].

[64] L. L. Frankfurt and M. I. Strikman, Comment on the west correction to the total cross-section, Phys. Lett. B **64** , 433 (1976).

[65] R. L. Jaffe, Deep inelastic scattering with application to nuclear targets, mIT-CTP-1261, Published in: Los Alamos Wkshp.1985:0537, Contribution to: Research Program at CEBAF (I).

[66] L. Frankfurt and M. Strikman, On the normalization of nucleus spectral function and the EMC effect, Phys. Lett. **B183**, 254 (1987).

[67] S. Weinberg, Dynamics at infinite momentum, Phys. Rev. **150**, 1313 (1966).

[68] M. M. Sargsian and F. Vera, New Structure in the Deuteron, Phys. Rev. Lett. **130**, 112502 (2023), arXiv:2208.00501 [nucl-th].

[69] F. Vera and M. M. Sargsian, Electron scattering from a deeply bound nucleon on the light-front, Phys. Rev. C **98**, 035202 (2018), arXiv:1805.04639 [nucl-th].

[70] J. Collins, The non-triviality of the vacuum in light-front quantization: An elementary treatment, (2018), arXiv:1801.03960 [hep-ph].

[71] M. M. Sargsian, Selected topics in high energy semiexclusive electronuclear reactions, Int. J. Mod. Phys. **E10**, 405 (2001).

[72] M. Piarulli, L. Girlanda, R. Schiavilla, A. Kievsky, A. Lovato, L. E. Marcucci, S. C. Pieper, M. Viviani, and R. B. Wiringa, Local chiral potentials with Δ-intermediate states and the structure of light nuclei, Phys. Rev. **C94**, 054007 (2016).

[73] M. Piarulli *et al.*, Light-nuclei spectra from chiral dynamics, Phys. Rev. Lett. **120**, 052503 (2018).

[74] A. Gezerlis, I. Tews, E. Epelbaum, S. Gandolfi, K. Hebeler, A. Nogga, and A. Schwenk, Quantum Monte Carlo Calculations with Chiral Effective Field Theory Interactions, Phys. Rev. Lett. **111**, 032501 (2013), arXiv:1303.6243 [nucl-th].

[75] A. Gezerlis, I. Tews, E. Epelbaum, M. Freunek, S. Gandolfi, K. Hebeler, A. Nogga, and A. Schwenk, Local chiral effective field theory interactions and quantum Monte Carlo applications, Phys. Rev. C **90**, 054323 (2014).

[76] I. Tews, S. Gandolfi, A. Gezerlis, and A. Schwenk, Quantum Monte Carlo calculations of neutron matter with chiral three-body forces, Phys. Rev. C **93**, 024305 (2016), arXiv:1507.05561 [nucl-th].

[77] B. S. Pudliner, V. R. Pandharipande, J. Carlson, and R. B. Wiringa, Quantum Monte Carlo calculations of A <= 6 nuclei, Phys. Rev. Lett. **74**, 4396 (1995), arXiv:nucl-th/9502031.

[78] S. C. Pieper, The Illinois Extension to the Fujita-Miyazawa Three-Nucleon Force, AIP Conf. Proc. **1011**, 143 (2008).

[79] J. Carlson, S. Gandolfi, F. Pederiva, S. C. Pieper, R. Schiavilla, K. E. Schmidt, and R. B. Wiringa, Quantum Monte Carlo methods for nuclear physics, Rev. Mod. Phys. **87**, 1067 (2015).

[80] J. Carlson, J. Morales, V. R. Pandharipande, and D. G. Ravenhall, Quantum Monte Carlo calculations of neutron matter, Phys. Rev. C **68**, 025802 (2003), arXiv:nucl-th/0103045.

[81] A. Lovato, J. Carlson, S. Gandolfi, and S. C. Pieper, Neutral weak response of neutron matter, Phys. Rev. C **91**, 062501 (2015), arXiv:1501.01981 [nucl-th].

[82] A. Lovato, S. Gandolfi, J. Carlson, N. Rocco, and E. Lusk, Quantum Monte Carlo calculation of neutral-current ν-^{12}C inclusive quasielastic scattering, Phys. Rev. C **97**, 022502 (2018), arXiv:1611.03605 [nucl-th].

[83] A. Lovato, J. Carlson, S. Gandolfi, N. Rocco, and R. Schiavilla, Electromagnetic and neutral-weak response functions of ^{4}He and ^{12}C, Phys. Rev. C **100**, 035502 (2019), arXiv:1711.02047 [nucl-th].

[84] A. Raghavan, A. Lovato, N. Rocco, and J. Carlson, Machine learning techniques for the inversion of the Laplace transform, Phys. Rev. Res. **2**, 043349 (2020), arXiv:2003.00956 [nucl-th].

[85] A. Lovato, S. Gandolfi, R. Butler, J. Carlson, E. Lusk, S. C. Pieper, and R. Schiavilla, Charge Form Factor and Sum Rules of Electromagnetic Response Functions in ^{12}C, Phys. Rev. Lett. **111**, 092501 (2013), arXiv:1305.6959 [nucl-th].

[86] N. Rocco, W. Leidemann, A. Lovato, and G. Orlandini, Relativistic effects in ab-initio electron-nucleus scattering, Phys. Rev. C **97**, 055501 (2018), arXiv:1801.07111 [nucl-th].

[87] A. Lovato, J. Carlson, S. Gandolfi, N. Rocco, and R. Schiavilla, Ab initio study of $(\boldsymbol{\nu_\ell}, \boldsymbol{\ell^-})$ and $(\boldsymbol{\overline{\nu}_\ell}, \boldsymbol{\ell^+})$ inclusive scattering in ^{12}C: confronting the MiniBooNE and T2K CCQE data, Phys. Rev. X **10**, 031068 (2020), arXiv:2003.07710

[nucl-th].

[88] A. Nikolakopoulos, A. Lovato, and N. Rocco, Relativistic effects in Green's function Monte Carlo calculations of neutrino-nucleus scattering, Phys. Rev. C **109**, 014623 (2024), arXiv:2304.11772 [nucl-th].

[89] A. Lovato, A. Nikolakopoulos, N. Rocco, and N. Steinberg, Lepton–Nucleus Interactions within Microscopic Approaches, Universe **9**, 367 (2023), arXiv:2308.00736 [nucl-th].

[90] K. S. Egiyan *et al.* (CLAS), Measurement of 2- and 3-nucleon short range correlation probabilities in nuclei, Phys. Rev. Lett. **96**, 082501 (2006), arXiv:nucl-ex/0508026.

[91] R. Weiss, A. W. Denniston, J. R. Pybus, O. Hen, E. Piasetzky, A. Schmidt, L. B. Weinstein, and N. Barnea, Extracting the number of short-range correlated nucleon pairs from inclusive electron scattering data, Phys. Rev. C **103**, L031301 (2021), arXiv:2005.01621 [nucl-th].

[92] O. Hen *et al.*, Momentum sharing in imbalanced Fermi systems, Science **346**, 614 (2014), arXiv:1412.0138 [nucl-ex].

[93] N. Fomin *et al.*, New measurements of high-momentum nucleons and short-range structures in nuclei, Phys. Rev. Lett. **108**, 092502 (2012), arXiv:0705.0159 [nucl-ex].

[94] I. Korover *et al.* (CLAS), 12C(e,e'pN) measurements of short range correlations in the tensor-to-scalar interaction transition region, Phys. Lett. B **820**, 136523 (2021), arXiv:2004.07304 [nucl-ex].

[95] VMC two-body momentum distributions, Quantum monte carlo results for two-nucleon momentum distributions, `https://www.phy.anl.gov/theory/research/momenta2/`.

[96] O. Benhar, A. Fabrocini, S. Fantoni, and I. Sick, Spectral function of finite nuclei and scattering of GeV electrons, Phys. Lett. B **219**, 29 (1989).

[97] R. M. Sealock *et al.*, Electroexcitation of the $\Delta(1232)$ in nuclei, Phys. Rev. Lett. **62**, 1350 (1989).

[98] P. Barreau *et al.*, Deep inelastic electron scattering from ^{12}C, Phys. Lett. B **126**, 475 (1983).

[99] O. Benhar, N. Farina, H. Nakamura, M. Sakuda, and R. Seki, Electron- and neutrino-nucleus scattering in the impulse approximation regime, Phys. Rev. D **72**, 053005 (2005), arXiv:nucl-th/0607029.

[100] R. Cruz-Torres *et al.* (Jefferson Lab Hall A Tritium), Comparing proton momentum distributions in $A = 2$ and 3 nuclei via ^{2}H ^{3}H and ^{3}He $(e, e'p)$ measurements, Phys. Lett. B **797**, 134890 (2019), arXiv:1902.06358 [nucl-ex].

[101] R. Cruz-Torres *et al.* (Jefferson Lab Hall A Tritium), Probing Few-Body Nuclear Dynamics via ^{3}H and ^{3}He $(e, e'p)$pn Cross-Section Measurements, Phys. Rev. Lett. **124**, 212501 (2020), arXiv:2001.07230 [nucl-ex].

[102] L. Andreoli, J. Carlson, A. Lovato, S. Pastore, N. Rocco, and R. B. Wiringa, Electron scattering on A=3 nuclei from quantum Monte Carlo based approaches, Phys. Rev. C **105**, 014002 (2022), arXiv:2108.10824 [nucl-th].

[103] L. Andreoli, G. B. King, S. Pastore, M. Piarulli, J. Carlson, S. Gandolfi, and R. B. Wiringa, Quantum Monte Carlo calculations of electron scattering from C12 in the short-time approximation, Phys. Rev. C **110**, 064004 (2024), arXiv:2407.06986 [nucl-th].

[104] A. Schmidt *et al.* (CLAS), Probing the core of the strong nuclear interaction, Nature **578**, 540 (2020), arXiv:2004.11221 [nucl-ex].

[105] R. Cruz-Torres *et al.*, Many-Body Factorization and Position-Momentum Equivalence of Nuclear Short-Range Correlations, Nature Physics **17**, 306 (2020), arXiv:1907.03658 [nucl-th].

[106] R. Weiss, A. W. Denniston, J. R. Pybus, O. Hen, E. Piasetzky, A. Schmidt, L. B. Weinstein, and N. Barnea, Extracting the number of short-range correlated nucleon pairs from inclusive electron scattering data, Phys. Rev. C **103**, L031301 (2021), arXiv:2005.01621 [nucl-th].

[107] E. R. Anderson, S. K. Bogner, R. J. Furnstahl, and R. J. Perry, Operator Evolution via the Similarity Renormalization Group I: The Deuteron, Phys. Rev. C **82**, 054001 (2010), arXiv:1008.1569 [nucl-th].

[108] S. Bogner and D. Roscher, High-momentum tails from low-momentum effective theories, Phys. Rev. C **86**, 064304 (2012), arXiv:1208.1734 [nucl-th].

[109] A. J. Tropiano, S. K. Bogner, R. J. Furnstahl, and M. A. Hisham, Quasi-deuteron model at low renormalization group resolution, Phys. Rev. C **106**, 024324 (2022), arXiv:2205.06711 [nucl-th].

[110] M. A. Hisham, R. J. Furnstahl, and A. J. Tropiano, Renormalization group evolution of optical potentials: Explorations using a "toy" model, Phys. Rev. C **106**, 024616 (2022), arXiv:2206.04809 [nucl-th].

[111] A. J. Tropiano, S. K. Bogner, R. J. Furnstahl, M. A. Hisham, A. Lovato, and R. B. Wiringa, High-resolution momentum distributions from low-resolution wave functions, Phys. Lett. B **852**, 138591 (2024), arXiv:2402.00634 [nucl-th].

[112] O. Artiles and M. M. Sargsian, Multinucleon short-range correlation model for nuclear spectral functions: Theoretical framework, Phys. Rev. **C94**, 064318 (2016), arXiv:1606.00468 [nucl-th].

[113] N. Fomin, D. Higinbotham, M. Sargsian, and P. Solvignon, New Results on Short-Range Correlations in Nuclei, Ann. Rev. Nucl. Part. Sci. **67**, 129 (2017), arXiv:1708.08581 [nucl-th].

[114] M. M. Sargsian, D. B. Day, L. L. Frankfurt, and M. I. Strikman, Searching for three-nucleon short-range correlations, Phys. Rev. C **100**, 044320 (2019), arXiv:1910.14663 [nucl-th].

[115] D. B. Day, L. L. Frankfurt, M. M. Sargsian, and M. I. Strikman, Toward observation of three-nucleon short-range correlations in high-Q2 A(e,e')X reactions, Phys. Rev. C **107**, 014319 (2023), arXiv:1803.07629 [nucl-th].

[116] Z. Ye *et al.* (Hall A), Search for three-nucleon short-range correlations in light nuclei, Phys. Rev. **C97**, 065204 (2018), arXiv:1712.07009 [nucl-ex].

[117] K. Egiyan *et al.* (CLAS Collaboration), Measurement of 2- and 3-nucleon short range correlation probabilities in nuclei, Phys. Rev. Lett. **96**, 082501 (2006).

[118] S. Li, S. N. Santiesteban, J. Arrington, R. Cruz-Torres, L. Kurbany, *et al.*, Inclusive studies of two- and three-nucleon short-range correlations in ^{3}h and ^{3}he (2024), arXiv:2404.16235 [nucl-ex].

[119] J. Ryckebusch, D. Debruyne, and W. Van Nespen, Polarization degrees of freedom in photoinduced two nucleon knockout

from finite nuclei, Phys. Rev. C **57**, 1319 (1998), arXiv:nucl-th/9710003.

[120] C. Colle, O. Hen, W. Cosyn, I. Korover, E. Piasetzky, J. Ryckebusch, and L. B. Weinstein, Extracting the mass dependence and quantum numbers of short-range correlated pairs from $A(e, e'p)$ and $A(e, e'pp)$ scattering, Phys. Rev. C **92**, 024604 (2015), arXiv:1503.06050 [nucl-th].

[121] R. Weiss, A. Lovato, and R. B. Wiringa, Isospin-symmetry implications for nuclear two-body distributions and short-range correlations, Phys. Rev. C **106**, 054319 (2022), arXiv:2206.14235 [nucl-th].

[122] W. Cosyn and J. Ryckebusch, Phase-space distributions of nuclear short-range correlations, Phys. Lett. B **820**, 136526 (2021), arXiv:2106.01249 [nucl-th].

[123] I. Tanihata, Effects of tensor interactions in nuclei, in *Handbook of Nuclear Physics*, edited by I. Tanihata, H. Toki, and T. Kajino (Springer Nature Singapore, Singapore, 2020) pp. 1–26.

[124] S. Terashima *et al.*, Dominance of tensor correlations in high-momentum nucleon pairs studied by (p,pd) reaction, Phys. Rev. Lett. **121**, 242501 (2018), arXiv:1811.02118 [nucl-ex].